Molecular mechanisms and physiological responses of rice leaves co-exposed to submicron-plastics and cadmium : implication for food quality and security

Molecular Mechanisms and Physiological Responses of Rice Leaves Co-exposed to Submicron-Plastics and Cadmium: Implication for Food Quality and Security

Xiang Wu [a, b], Shanshan Yin[e], Yao Liu[f], Yuwei Zhu[a, c], Timing Jiang[a, c], Sha Liang[a, c], Shijie Bian[a, c], Yaowu Cao[b], Guojing Wang[b], Jiakuan Yang[*, a, c, d]

a *School of Environmental Science & Engineering, Huazhong University of Science & Technology, Wuhan, Hubei, 430074, China*

b *School of Resources and Environmental Science, Hubei University, Wuhan 430062, China*

c *Hubei Provincial Engineering Laboratory of Solid Waste Treatment, Disposal and Recycling, Wuhan, Hubei, 430074, China*

d State Key Laboratory of Coal Combustion, Huazhong University of Science & Technology, Wuhan, Hubei, 430074, China

e Toxicological Center, Universiteit Antwerpen, Universiteitsplein 1, Wilrijk 2610, Belgium

f College of Environmental and Biological Engineering, Wuhan Technology and Business University, Wuhan, Hubei, 430065, China

[*] **Corresponding author:** Prof. Jiakuan Yang
Email addresses: jkyang@mail.hust.edu.cn; yjiakuan@hotmail.com
Tel: +86-27-87540995; Fax: +86-27-87792207

Abstract

The effects of co-exposure to aged submicron particles (aSMPs) and Cd as model contaminants on rice leaves via the foliar route were investigated. Thirty-day-old rice seedlings grown in soil were exposed to Cd (nitrate) through foliar spraying at concentrations of 1, 10, 50, 100, and 500 uM, with or without aSMP at a rate of 30 μg d^{-1}. It was observed that Cd translocated from leaves to roots via stems even without co-exposure to SMP. Co-exposure can reduce cadmium levels in leaves. Laser ablation inductively coupled plasma mass spectrometry (LA-ICP-MS) analysis confirmed a significant reduction (29.3 − 77.9%) in Cadmium accumulation in the leaves of rice plants during co-exposure. Exposure to Cd resulted in physiological, transcriptomic, and metabolomic changes in rice leaves, disrupting 28 metabolism pathways, and impacting crop yield and quality. Exposure to both Cd and aSMPs can interfere with the Cd distribution in plants. Rice leaves exposed solely to Cd exhibit higher toxicity and Cd accumulation, compared to those co-exposed to Cd and aSMPs. The accumulation of Cd in plant leaves is enhanced with aSMPs, which may lead to more pronounced gene expression regulation and changes in metabolic pathways, compared to Cd exposure. Our study found that the independent Cd exposure group had higher Cd accumulation and toxicity in rice leaves compared to the combined exposure of Cd and aSMPs. We hypothesize that aged negatively charged SMPs can capture Cd and reduce its exposure in the free state while jointly inhibiting Cd-induced oxidative and chloroplast damage, thereby reducing the potential risk of Cd exposure in rice plants.

Environmental Implication

Investigating the co-exposure to aged Submicron Plastics (aSMPs) and Cadmium (Cd) is imperative given their documented environmental hazards. This research seeks to elucidate the combined toxic effects on rice growth. The results are expected to improve our understanding of the fate and effects of aSMPs, while facilitating the development of mitigating strategies. Furthermore, it highlights plant responses to the co-occurrence of aged microplastics and atmospheric Cd, highlighting potential environmental risks in agricultural contexts. In the presence of these hazardous materials, this research serves as a critical step in protecting plant and human well-being.

Keywords: Foliar pathway; co-exposure; Transcriptome; Metabolome.

1. Introduction

The contamination of agricultural and food-producing land has emerged as a significant global environmental and food security concern, as approximately 64% of such land is currently at risk of contamination (Tang et al., 2021). The pattern of contamination has evolved from localized, single contaminant-dominated contamination to a regional, persistent, multi-contaminant co-exposure scenario (Sun et al., 2018). Accumulation and transfer of contaminants in the crop through the food chain poses a significant threat to human (Liu et al., 2010; Zeb et al., 2022). With the global food demand expected to increase by at least 50% by 2050, ensuring food security has become a major challenge for humanity (Liu et al., 2021). However, pollution caused by the deposition of atmospheric contaminants, such as metal ions and microplastics, is more widespread and complex than terrestrial pollution (Revell et al., 2021). Some of these contaminants are absorbed by leaves and accumulate in plants, while others are deposited in soils and taken up by roots, ultimately contaminating crops (Chiaia-Hernandez et al., 2017). The global deposition and risk of these contaminants is often underestimated. Thus, the exposure of crops to atmospheric depositional contaminants cannot be ignored, making it a critical issue that needs to continue to be addressed.

As one of the most toxic contaminants in the environment, cadmium (Cd) poses a serious environmental threat to humans(Wang, J. et al., 2023). Cd can be absorbed by plants and accumulated in the edible part of the plant, resulting in reduced grain yield and food quality. It can also lead to chronic health effects in humans, such as liver and kidney damage, weakness, and an increased risk of other acute adverse health effects. Atmospheric deposition is a major source of Cd input to crops (up to 21%) (Li et al., 2021). In Asia, 30-84% of Cd is exchangeable. Because the activity of Cd in atmospheric deposition is higher than that in soil, Cd in air is more readily taken up by plants(Ouyang et al., 2023). It has become an important source of Cd accumulation in agricultural products in some regions(Jing et al., 2023). Zhang et al (Zhang et al., 2010) found a 153 % higher Cd content in airborne part of Chinese cabbage than in film-covered part by contrast test of atmospheric deposition exposure. Cd is toxic to plants via various pathway, including inhibiting photosynthesis and respiration, reducing water and nutrient uptake, and reducing biomass (31% in wheat at concentrations ranging

from 0.03 to 4.8 mM, and 100% in rice at 1.0 mM) (El Rasafi et al., 2020). Cd can affect photosynthesis (Hasan et al., 2009; Vassilev et al., 2002) by interfering with the enzyme activities, electronic photosynthetic transport, stomatal shrinkage, and reduces intercellular carbon dioxide concentration (Engineer et al., 2016). The adverse effects of Cd on photosynthesis are due to interference with chlorophyll, berry quinone and carotenoid synthesis, Calvin cycle enzyme activity and carbon dioxide fixation (Nikolić et al., 2014). However, current research is mainly focused on Cd induced physiological and molecular changes in plants, while studies on transport and toxic effects of co-occurring contaminants in atmospheric deposition are limited.

Microplastics are a newly recognized air pollutant. They've been found all over the world since they were first reported in 1972. Microplastic pollution has become a global environmental concern (Bi et al., 2020). Research on microplastic pollution has mainly focused on the aquatic environment (de Souza Machado et al., 2018) and the terrestrial environment(Xu et al., 2020), while microplastics in the atmospheric environment have recently gained more and more attention. Many studies have confirmed the presence of microplastics in the atmospheric system and emphasized the important contribution of atmospheric deposition even in (the most) remote areas (Revell et al., 2021; Zhang et al., 2019). It has been reported that microplastics can reach 175 to 313 particles/m^2/day in Dongguan (Cai et al., 2017), 0 to 4.18 particles/m^2/day in Shanghai (Liu, K. et al., 2019) and 2 to 355 particles/m^2/day in Paris (Dris et al., 2016). At a height of 1.5 m above the ground, airborne microplastics are mainly the result of dynamic process of settling and floating of the microplastics on the ground (Li et al., 2020). Terrestrial plants may play an important role in the fate of microplastics in the atmosphere, being considered as potential temporary sinks for microplastics during atmospheric transport (Liu et al., 2020). In addition, Zhou et al. (exposed to polystyrene microplastics at 0, 10, 50, and 100 mg L^{-1} for 16 d) confirmed that exposure to polystyrene microplastics would lead to oxidative stress and damage to the antioxidant system of rice (Zhou et al., 2021), which would significantly affect the growth of rice and reduce its nutritional quality. Similar plant toxicity of Microplastics also exists in lettuce (Lian et al., 2021) and wheat (Lian et al., 2020a). In addition, stomatal absorption and cuticle are considered as possible ways for plant leaves to absorb Microplastics (Lv et al., 2019; Wang et al., 2022b). The transport of microplastics absorbed

through plant stomata to other parts of the plant occurs *via* the exoplast pathway (Hong et al., 2014; Wang, Y. et al., 2023; Zhao et al., 2017), while the entry of microplastics into the plant primarily occurs through the cuticle, leading to accumulation in the leaves (Wang et al., 2022b). This phenomenon has been observed in various studies (foliar-exposed to Microplastics at 0, 0.1 and 1 mg L^{-1} and seed-exposed at 0-10 mg L^{-1} for 30 d) and has significant implications for the fate and effect of microplastics in plants (Lian et al., 2021; Lian et al., 2020a).Additionally, research has shown that exposure to polystyrene microplastics can induce oxidative stress and damage to the antioxidant system in plants such as rice, lettuce, and wheat, which may lead to reduced growth and nutritional quality (Lian et al., 2020b; Wu et al., 2022; Wu et al., 2020).These findings highlight the potential risks associated with microplastic pollution in the agricultural sector and the need for further research to develop effective mitigation strategies.

Microplastics also degrade and fragment, changing their physical and chemical properties when exposed to environmental factors such as sunlight, temperature, moisture, and biological processes (Liu, J. et al., 2019). This leads to plastic aging in the environment(Bhagat et al., 2022; Lu et al., 2023). The aging rate is much faster in the soil than in the aquatic environment (Zhang et al., 2021). Aging of (micro)plastics includes formation of surface cracks and fissures, release of chemical additives, and formation of new chemical functional groups such as O-functional groups (C-O, C-OH, and C=O) (Ding et al., 2020) on the plastic surface (Li et al., 2018; Velzeboer et al., 2014). Therefore, aged (micro)plastics, either through morphological changes or chemical groups on the surface, may pose a greater risk to the environment than newly released/commercialized (micro)plastics(Liu, P. et al., 2019). However, current studies mostly use “just manufactured” microplastics in the experiments, and the effects of aging in the microplastics are largely ignored (Wang et al., 2022b).

Based on the properties of aSMPs and Cd, the potential toxic effect of their co-exposure on rice growth requires further investigation. Plant cell walls exhibit varying charges due to the presence of carboxylic groups, potentially resulting in differential uptake of Cd and aSMPs by plants through the foliar pathway. In this study, we hypothesised that (1) co-exposure to Cd may affect Cd distribution in the plant, and (2) the increased

accumulation of Cd with aSMPs in plant leaves may lead to more pronounced regulation of gene expression and altered metabolic pathways than solely exposed to Cd.

This study evaluated Cd and SMP accumulation on rice leaves, determined Cd concentrations on rice leaves and roots, and assessed rice growth parameters, photosynthetic pigment concentrations, and antioxidant system. Furthermore, in order to identify the possible molecular mechanisms underlying the growth inhibition induced by the foliar exposure to Cd and aSMPs, we carried out transcriptomic and metabolomic analyses. The results of this study may improve our understanding of the effects and fate of SMPs and contribute to the development of strategies for the prevention and control of their effects. This research also highlights the potential environmental risks associated with microplastics in agricultural production by providing information on how plants respond to co-exposure to aSMPs and Cd in atmospheric deposition.

2. Materials and methods

2.1 Chemicals and Standards

Aged Submicron-plastic (PS-COOH, aSMPs) was purchased from BaseLine Co., Ltd. (Tianjin, China) and used without further modification. These SMPs, with an approximate diameter of 300 nm and an initial concentration of 10 mg mL^{-1} (w/v), were fluorescent red marked (excitation/emission wavelengths of 540/580 nm). Cd $(NO_3)_2$ was prepared at 1, 10, 50, 100, 500 μM. Concentrations of other ions in the MP suspension mother liquor do not exceed 1%, so it was assumed that other ions in the suspensions would not affect experimental results. PS-MP morphology was examined by high-resolution transmission electron microscopy (FSEM; TecnaiG2 F30, FEI Ltd., Netherlands) as described in Supporting Information (SI) (Figure S1 and Text S1).

2.2 Crop Cultivation and Exposure Treatments

Seeds of *Oryza sativa* L. hybrid indica 9108 rice plants (N9108) were purchased from Gaoke Horticulture Co., Ltd. (Jiangsu, China). The rice seeds were germinated. After 10 plants with similar growth trend were selected, they were moved into the soil to continue growing for 30 days.

To estimate the capacity of SMPs retained by rice leaves, a method previously described by Huang et al.

(Huang et al., 2015) was used. We modified Huang's estimation method for dust accumulation on plant leaves. The dust retention capacity of rice was calculated as follows:

Capacity of SMPs retained by plant leaves = dust retention capacity of plant × leaf area of plant × concentration of SMPs in dust.

Depending on the leaf size, the dust retention capacity of a rice plant under normal dust fall conditions is about 0.42 mg d^{-1}. Therefore, a dose of 30 μg d^{-1} of aSMPs was used as the exposure dose for each rice plant. This dose could represent the actual deposition of aSMPs based on the median MP count in Chinese cities (Liu, C. et al., 2019; Lu et al., 2020). Cd fluxes in dust were used to estimate Cd deposition on rice leaves, and exposure doses ranging from 1 to 500 μM d^{-1} were assumed for each rice plant to represent potential and extreme deposition levels of Cd. The wet deposition method was used for the study and the experimental method for foliar exposure to nanoparticles as described by Xiong et al., (Xiong et al., 2017) was applied. The droplets of SMPs suspension and Cd were applied to the adaxial surface of rice leaves using a pipette. The treatments were replicated eight times, and dry sponge mats were placed to avoid root contact with SMPs and Cd. Experiments were conducted in an artificial climate chamber with a 16/8h light/dark cycle, 28/22°C temperature cycle and 70%/30% relative humidity cycle. Rice leaf samples were collected and further evaluated after 30 days.

2.3 *In-situ* Quantification of Cd in Rice leaves

The *in-situ* quantification of Cd in rice leaves was carried out using laser ablation inductively coupled plasma mass spectrometry (LA-ICP-MS) on an ArF excimer 193 nm laser ablation system, coupled to a quadrupole ICP-MS (Agilent 7700x, Agilent Technologies, Inc., USA). The rice leaves were placed under the laser and burned with a spot size of 90 microns. Each LA-ICP-MS analysis involved a background acquisition step of 20 s to ensure accurate quantitative measurements. Further details can be found in the SI (Text S2)

2.4. Characterization of MP and Cd Accumulation

The intact rice leaves from different treatments were cut perpendicular to the main leaf vein for cross-sectional observation using a Leica Laser Scanning Confocal Microscope (LSCM). The excitation/emission

wavelengths of 540/580 nm were used for aSMPs observation. After that, the sections were stained with a Cd-specific fluorescent probe (Leadmium TM Green AM dye) and left in the dark for 75 minutes. The distribution of Cd was observed using LSCM with excitation/emission wavelengths of 488/515 nm.

2.5 Growth and Physiological Responses of Rice Plants

Several parameters, including plant height, number and fresh weight of leaves, and length and fresh weight of roots, were determined to assess rice growth. Plant height was measured prior to the separation of the roots and leaves. Fluorescence parameters and photosynthetic efficiency were measured using a pulse-amplitude modulated fluorophotometer (Walz, Germany) on rice leaves collected from both control and pesticide-treated groups after 15 min of shade. Fresh leaves and roots were weighed after washing with distilled water and drying.

For biochemical analysis, leaf samples weighing 0.2 g were frozen in liquid nitrogen and ground to a fine powder. The powder was then transferred to centrifuge tubes containing 2 mL of extract. The supernatants were collected in 10ml tubes. Assay kits from Meimian Biotechnology Co., Ltd., China, were used to measure reactive oxygen species (ROS) levels and the activity of superoxide dismutase (SOD), catalase (CAT) and peroxidase (POD). Further details can be found in the SI (Text S4).

2.6 Metabolomics Analysis

Briefly, for the metabolomics analysis, grains from each group were dried in an oven for 36 hours until the water content reached 12 -14 wt%. The dried grains were stored at room temperature for 3 months before being used for the analysis of nontarget metabolites by gas chromatography-mass spectrometry (GC-MS) using an Agilent 7890B-5977B. Metabolic pathway analysis was performed using MetaboAnalyst 5.0 (Pang et al., 2022) based on the GC-MS data. More information about the GC-MS analysis, including extraction and instrument parameters, can be found in the SI (Text S5).

2.7 RNA-sequencing and Validation by RT-qPCR

RNA-seq analysis was carried out at Novogene Biotech Co., Ltd. Total RNA was extracted from ground grains, and a transcriptome library was prepared using 1 μg of total RNA. The library was sequenced on an Illumina

NovaSeq platform, and 150 bp paired-end reads were generated. Protein databases (KEGG, Pfam, and GO) were used to annotate the unigenes. Real-time quantitative PCR was used to validate the transcriptomic data using the heterogeneous nuclear ribonucleoprotein (HNR) as the internal reference gene. The RT-qPCR amplification program was run for 40 cycles, and specific primers were designed using Primer BLAST. Details are provided in the SI (Text S6 and Table S4).

2.8 Statistical Analysis

All biochemical analyses were conducted using six replicates for each treatment. Nine cDNA libraries were generated from the three replicates of rice exposed to various conditions. The normal distribution of the data was assessed using the Kolmogorov–Smirnov (K–S) test. For comparisons between groups, one-way analysis of variance (ANOVA) followed by the least-significant difference (LSD) test was used. SPSS Statistics 18.0 (IBM, New York) was utilized for statistical analysis, and statistical significance was considered at $p < 0.05$.

3. Results

3.1 Biological Responses of the Rice Leaves

Both co-exposure and solely exposed to Cd groups significantly affected the biomass of rice, including plant height, number of leaves and fresh weights of leaves and roots ($p < 0.05$) (Figure S3 and Figure 1A-D). However, there was no significant difference in the growth of rice due to the treatment of aSMPs without the exposure to Cd (Figure 1A-D). The effect of the microplastics on the growth of the rice plants was also not significantly different from that of the foliar application of co-exposure to Cd and aSMPs. Although more Cd accumulated on the rice leaves in the higher Cd exposure groups co-exposed with aSMPs, there was no significant difference between the growth parameters of the different Cd exposure levels. Following foliar exposure to Cd/aSMP co-exposure and solely exposed to Cd, the chlorophyll content of rice leaves decreased, and the same trend was observed for the carotenoid content and net photosynthetic rate of rice leaves. (Figure 1 E-H). The activities of CAT, POD and SOD (Figure 1 I-K) increased with Cd concentration but did not exceed the tolerance of rice leaves. In particular, the activity of CAT in the leaves was more affected by Cd exposure only than co-exposure groups (Figure 1I). The level of γH2AX, an indicator of DNA damage,

increased with increasing Cd levels. Foliar exposure to both Cd only exposure and co-exposure to Cd and SMPs can significantly increase the levels of MDA and ROS in rice leaves, thereby inducing a lipid peroxidation stress response (Figure 1M, N). With increasing Cd exposure concentration, the total cell membrane permeability increased in leaves and roots without SMPs treatment, while it increased in leaves but had no significant difference in roots with SMPs treatment. (Figure 1O, P).

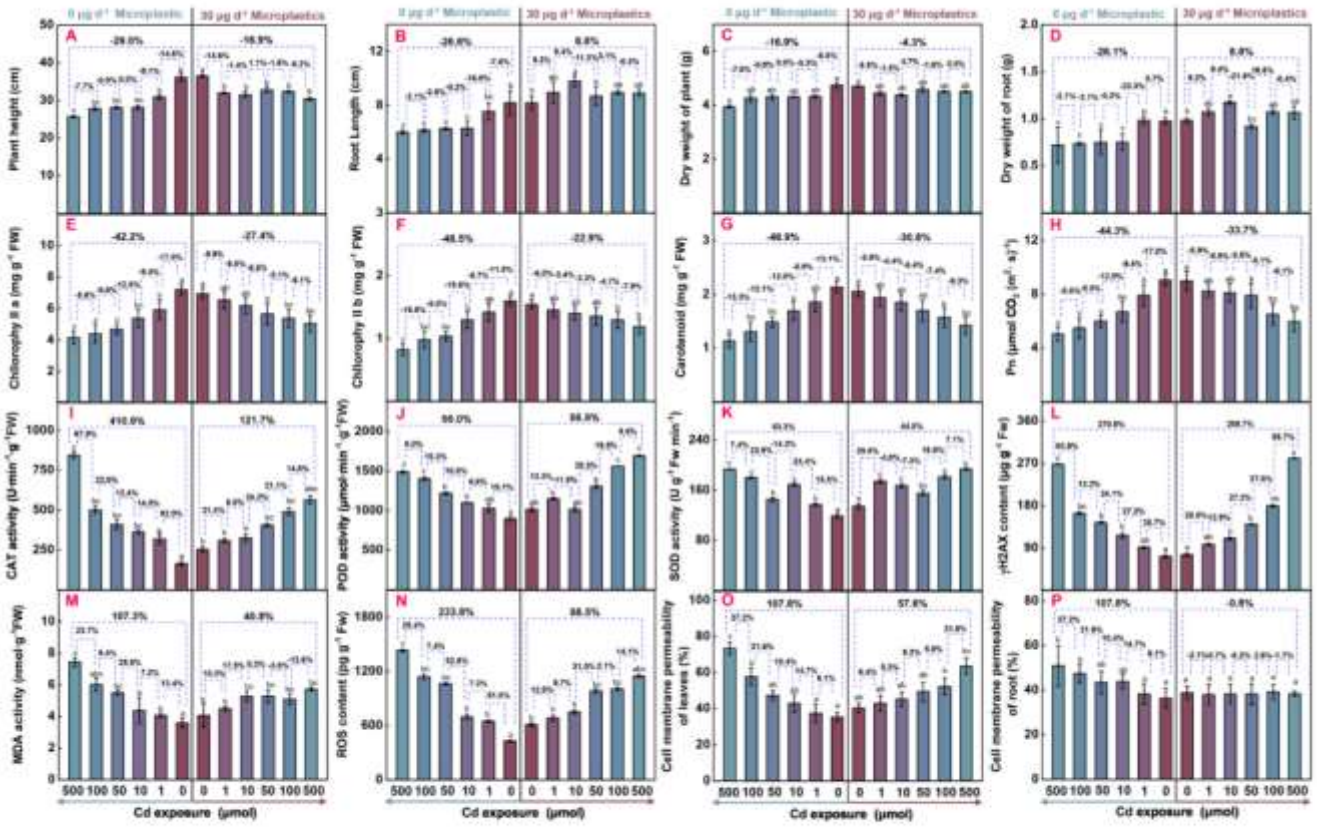

Fig. 1. Plant height (A), root length (B), dry weight of plant (C) and root (D), and the chlorophyll a (E), chlorophyll b (F), carotenoid(G), photosynthetic efficiency (H), catalase (CAT, I), peroxidase (POD, J) and superoxide dismutase (SOD, K) activity, γH2AX (L), malonic dialdehyde (MDA,M), and reactive oxygen species (ROS, N), cell membrane permeability of leaves (O) and root (P) in rice leaves following foliar exposure to differentially charged Cd with/without aSMPs. Different lowercase letters indicate significant differences between the different treatments ($p < 0.05$). The percentage figures show the magnitude of change between the different treatment groups (0/1 μM, 1/10 μM, 10/100 μM, 100/500 μM and 0/500 μM, with/without aSMPs).

3.2 Cd and SMPs in the Rice Leaves

The results showed a significant reduction ($p < 0.05$) in Cd accumulation in rice leaves after foliar spraying of aSMPs (Figure. 2 and 3C). The images from laser scanning confocal microscopy (LSCM) and laser ablation inductively coupled plasma mass spectrometry (LA-ICP-MS) indicated that there were no Cd signals in rice leaves with no Cd exposure group, while higher levels of Cd treatment resulted in more Cd accumulation in leaves (Figure 2) and more intense fluorescence signals in the leaf cross section (Figure 3A a,b,c,d,e,f). However, in the SMP co-exposure scenarios, Cd accumulation in rice leaves was reduced by 29.3 to 77.9%,

and the fluorescence signals of Cd were mainly distributed along the leaf vascular bundles (Figure 3B h-l, n-r and t-x). In contrast, the treatment group with foliar spray of aSMPs showed Cd accumulation mainly along the leaf vascular bundles (Figure 3A b,c,d,e,f). Additionally, the Cd concentrations in rice leaves and roots were measured to verify the effect of aSMPs on Cd accumulation in rice. The results showed that Cd concentrations in leaves without SMPs treatment were 4.51, 1.93, 1.84, 1.75, and 1.41 times higher than those in SMP-treated leaves for 1, 10, 50, 100, and 500 μM Cd, respectively. No microplastics were detected in the roots of all treatments, and Cd was detected only in the roots without SMPs treatment.

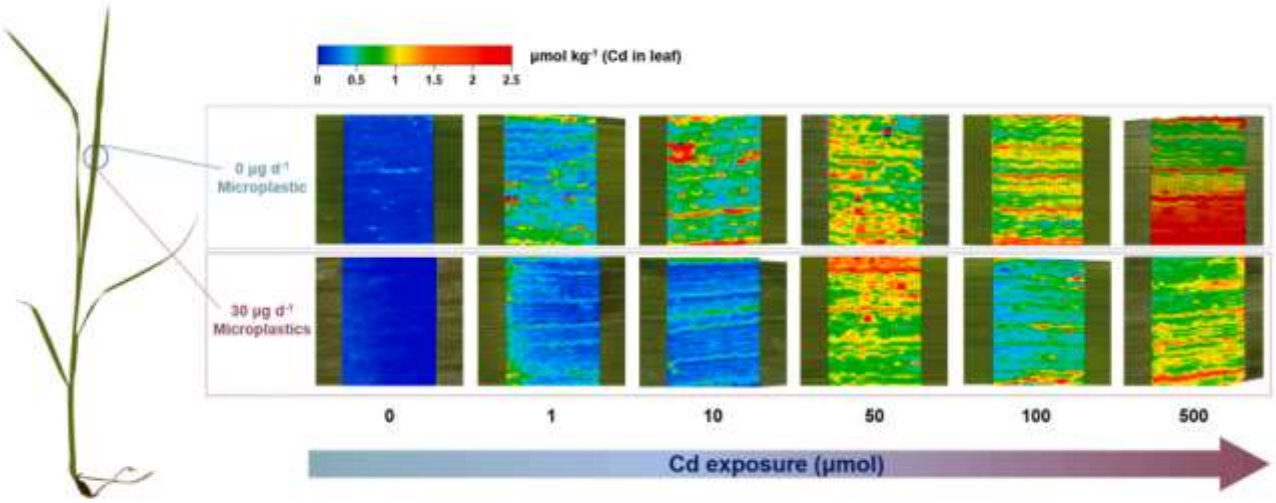

Fig. 2. *In-situ* quantification of Cd in rice leaves by LA-ICP-MS. Foliar spray of 0,1,10,50,100 and 500 μM Cd exposure joint 0 μg d^{-1} microplastic and 30 μg d^{-1} microplastics.

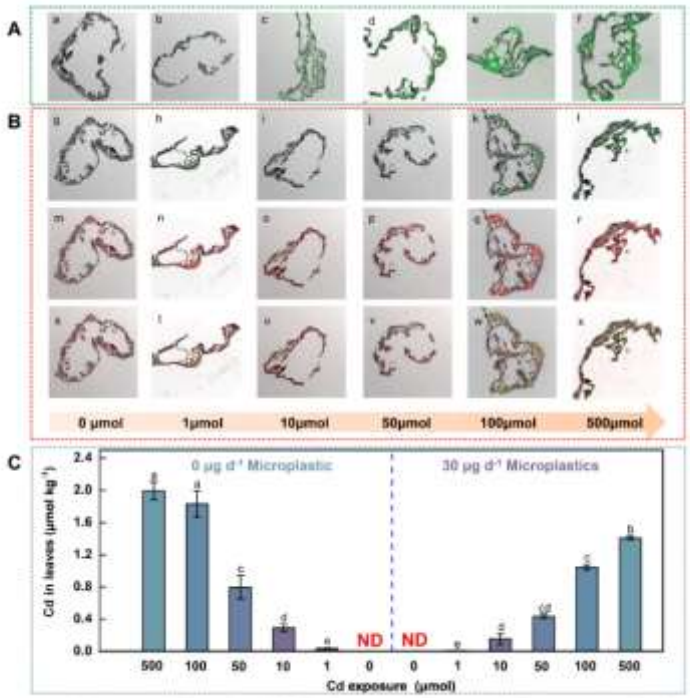

Fig. 3. Laser scanning confocal microscopy (LSCM) images (A, B) of rice leaf cross section with foliar exposure to different treatments. A (a-f) and B (g-l) was Cd in rice leaf cross section foliar spray of 0, 1, 10, 50, 100 and 500 μM Cd exposure joint 0 and 30 μg d^{-1} microplastic. B (m, n, o, p, q, r) was MPs in rice leaf cross section foliar spray of 0, 1, 10, 50, 100 and 500 μM Cd exposure. B (s-x) is the superposition of Cd and MPs fluorescence. (C) Cd concentrations (μM kg^{-1}, dry weight) in rice leaves foliarly exposed to different treatments.

3.3 Transcriptomic Analysis of Rice Leaves

Cd with aSMPs treatment showed a higher effect on the regulation of gene expression in rice leaves than Cd without aSMPs treatment (Figure S5). Compared to the group without Cd exposure, differentially expressed genes (DEGs) increased with increasing Cd levels: 2769 (1 μM Cd), 3762 (10 μM Cd), 3146 (50 μM Cd), 3315 (100 μM Cd), and 4123 (500 μM Cd) without aSMPs treatment (Figure S6 A a, b, c, d, e), and 4693, 3279, 4519, 3154, and 3594 genes with aSMPs treatment (Figure S6 B f, g, h, i, j), respectively. Under the stress of Cd without aSMPs, the number of down-regulated DEGs was higher than the number of up-regulated DEGs at different levels of Cd, and the amount of up- and down-regulated DEGs increased with increasing levels of Cd. (Figure S6 A, a-e). On the contrary, the number of up-regulated DEGs was higher than down-regulated DEGs at different Cd levels in aSMPs (Figure S6 B, f-j). Functional GO annotation of the DEGs revealed that in all Cd treatments, the highest number of up- and down-regulated DEGs were found in oxidoreductase activity (MF), photosystem (CC) and cellular response to stimulation (BP) (Figure S7 A, B). The number of DEGs in most GO terms upon different levels of Cd with aSMPs treatment exposure was higher than in different levels of Cd without SMPs treatment. KEGG enrichment analyses showed that DEGs belonging to Cd exposure without aSMPs (Figure S7A and S8A) and Cd exposure with aSMPs (Figure S7B and S8B) treatments caused the enrichment of 28 metabolism pathways, including citrate cycle (TCA cycle), photosynthesis, carbon metabolism, pyruvate metabolism, and amino sugar and nucleotide sugar metabolism. In addition, DEGs associated with Cd exposure without aSMPs were significantly enriched in fructose and mannose metabolism, circadian rhythm (plant), sulfur metabolism, glyoxylate and dicarboxylate metabolism, alanine, aspartate and glutamate metabolism and diterpenoid biosynthesis. Pantothenate and CoA biosynthesis, cutin, suberine and wax biosynthesis, fatty acid degradation, glycerolipid metabolism, and photosynthesis (antenna proteins) were significantly enriched by DEGs belonging to Cd exposure with aSMPs. The results of RT-qPCR and transcriptomic analysis showed a significant correlation ($p < 0.01$) between the Cd exposure only and Cd exposure with aSMPs treatments (Figure S9A, B), suggesting the accuracy of the transcriptomic data.

3.4 Metabolic Alterations Induced by Cd in Rice Leaves

A total of 109 metabolites in rice grains were identified based on a specific criterion, with 91 metabolites found to be common among the different exposure groups and ithcultivars (Figure S4). Using OPLS-DA (VIP > 1, $p < 0.05$), the differential metabolites in each treatment were identified (Table S1 and S2). Among the shared metabolites, 70.7% had potential impacts on rice quality, such as head rice yield, amylose content, and protein content. Principal Component Analysis (PCA) and Orthogonal Partial Least Squares Discriminant Analysis (OPLS-DA) were used to analyze the differential metabolic changes caused by different levels of Cd exposure with/without aSMPs treatment. The resulting plot (Figure 4 b, e) showed that the group without the Cd exposure clustered together with the 1, 10, 50, 100, 500 μM Cd exposure groups along PC1 (71.5%) and PC2 (43.2%) for treatment without aSMPs, and along PC1 (69.2%) and PC2 (28.2%) for treatment with aSMPs, while group without the Cd exposure was clearly separated from the 1, 10, 50, 100, 500 μM Cd exposure groups. Amino acids, carbohydrates, and lipids were found to be the main metabolites that were different from the without Cd exposure group in both treatments (Figure 4 c, f). The different Cd levels with/without aSMPs treatment had significant effects on some metabolic pathways (Figure 4 a, d). Cd exposure without aSMPs affected alanine, aspartate and glutamate metabolism and fructose and mannose metabolism (Figure 4a), while Cd exposure with aSMPs affected pantothenate and CoA biosynthesis, cutin, suberine, and wax biosynthesis (Figure 4 b). The metabolism of porphyrins and chlorophyll was found to be enriched in the leaves of all Cd treatments, indicating that it played an important role in the response to Cd-induced stress. Most of the metabolites involved in the porphyrin and chlorophyll metabolism were decreased in the Cd exposure without aSMPs, whereas they were increased in the Cd exposure with aSMPs compared to the control (Figure 4 a, d).

4. Discussion

Commercial plastic particles tend to agglomerate as they approach the nanometer scale (Lian et al., 2020b). In this study, through various ageing processes simulating the environmental behaviour of the plastics, carboxyl groups was introduced to the surface of the aSMP spheres. The size and electrical charge of the particles play a complex role in the bioavailability and toxicity of the particles (Huffer et al., 2019; Kalcikova

et al., 2017). These negatively charged plastic particles can promote their physical adsorption to plant roots and algae through electrostatic attraction, inhibiting photosynthesis or nutrient fixation (Kalcikova et al., 2017; Lian et al., 2020a; Wang et al., 2022b). Negatively charged particles have a strong affinity for heavy metals, which may be carried by these particles [48].

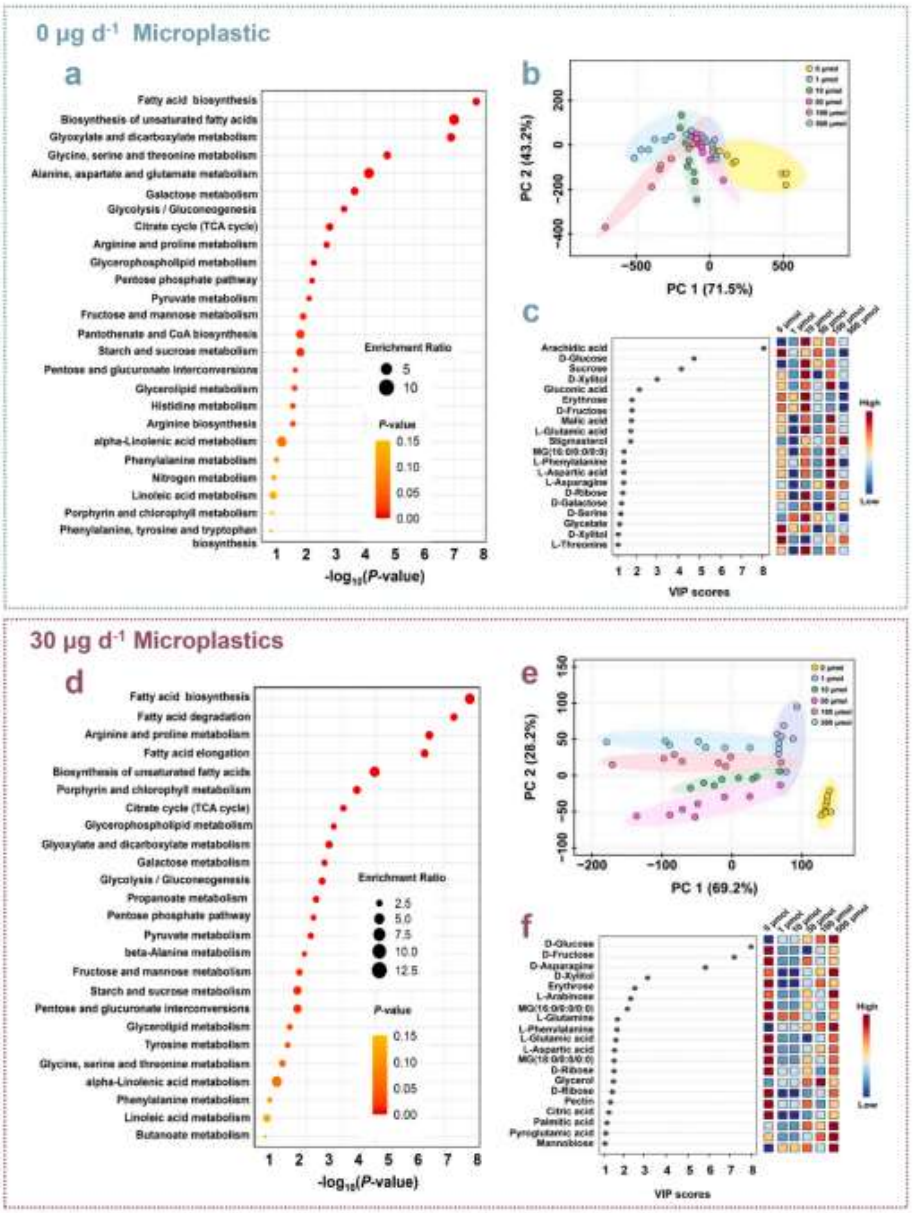

Fig. 4. Metabolic pathway enriched analysis of the differential metabolites in the treatments of 0, 1, 10, 50, 100 and 500 μM Cd exposure (a) and 0, 1, 10, 50, 100 and 500 μM Cd exposure with aSMPs (d), The abscissa coordinate represents the impact value of the metabolic pathway. The bubble size represents the number of metabolites. The vertical coordinate and bubble color represent the *p* value of enrichment analysis. Score scatter plot of principal components analysis (PCA) for identified differential metabolites under the 0, 1, 10, 50, 100 and 500 μM Cd exposure stress (b) and 0, 1, 10, 50, 100 and 500 μM Cd exposure with aSMPs stress(e). The scatter shape and color represent different experimental groups. PC1: first principal component score; PC2: orthogonal principal component score. Variable importance in projection (VIP) scores of the top 20 metabolites and relative pathway impacts analysis under 0, 1, 10, 50, 100 and 500 μM Cd exposure(c) and 0, 1, 10, 50, 100 and 500 μM Cd exposure with aSMPs stress(f).

It was found that these particles were able to enter the rice leaves *via* the stomata, while the positively charged particles accumulating in the epidermal cell wall of the leaf. This process may be a potential pathway for microplastics to enter plant (Figure 2B). Cd affected the gas exchange parameters of the plant, causing

stomatal closure and preventing further Cd uptake (Avellan et al., 2021; Perez-Romero et al., 2016). Our results indicated that the cadmium that was transported by the aSMP accumulated in the cross-sectional area of the rice leaves, but it was not transported to the other parts of the plant. In addition, strong bindings between the negatively charged aSMP and Cd made it difficult for the heavy metal to migrant in the plant (Figure 1). These two factors could explain the lowered Cd levels in the leaves of the co-exposure group for Cd and aSMPs.

Foliar exposure to Cd has been shown to have a negative effect on the growth of rice plants in this study (as shown in Figure 2 and S3). Results showed seed germination, early seedling growth and total plant biomass can be reduced by Cd exposure. It can also cause changes in critical physiological parameters of the plants, e.g., photosynthesis, relative water content, transpiration rate, stomatal conductance, and electrolyte leakage. These can result in a direct reduction in crop yield (Bae et al., 2016; Saleh et al., 2020; Soudek et al., 2014; Zouari et al., 2016). Previous reports indicate that aged polystyrene is electrically charged (either positive or negative) which could result in electrostatic adsorption of Cd (Wang et al., 2022a). However, in our study, compared with the group exposed to Cd alone, the co-exposure group Cd + aSMP did not show further decrease in photosynthetic pigments or their derivatives in rice leaves and no further decrease in photosynthetic efficiency too (as shown in Figure 3 E, F, G and H). Combine exposure to aSMP and higher level of Cd exposure (500) and low level of Cd exposure (1) both have adverse effect on rice parameters, indicating that foliar exposure to environmental relevant concentration of Cd and SMPs could cause rice growth inhibition.

Lipid peroxidation is a process that was known to damage the membrane structure essential for maintaining plant metabolism. Cd-induced lipid peroxidation presents a notable threat to plants (Guo et al., 2007; Rizwan et al., 2018). Furthermore, cadmium stress in plants can cause notable alterations in enzyme activity by inducing oxidative stress in plant cells (Gupta et al., 2019; Rellan-Alvarez et al., 2006). Carotenoids are light-absorbing pigments that absorb photons and transfer excitation energy to chlorophyll (Young, 1991). These pigments also act as potent quenchers of ROS (Shaw and Hossain, 2013) such as O^{2-} and H_2O_2 (Xiong et al.,

2021), which can damage chloroplast structure and inhibit photosynthetic activity, leading to a decrease in chlorophyll content (Green et al., 1991). The function of antioxidant enzymes such as SOD, POD and CAT is the removal of excess O_2 and H_2O_2 to reduce the effects of biotic or abiotic stress (Asada, 1992; Sengupta et al., 1993; Willekens et al., 1997).

In the co-exposure, results showed that the reduction in carotenoids was lower than the group exposed to Cd only, with about half of that decrease (as shown in Figure 3G). The elevated ROS levels in the combine exposure group was also found to be only one third to the value reported in the independent exposure to Cd only, indicating that carotenoids in the co-exposure group can effectively quench more reactive oxygen (as shown in Figure 3N). However, O^{2-} content and CAT activities showed slightly different pattern between the combined and individual exposure groups. Difference were only found to be significant in 1, 50 and 500 μM Cd groups (as shown in Figure 3 I and N). Similar results were also observed in rice roots exposure study to SMPs (Lian et al., 2020b; Wu et al., 2022; Wu et al., 2020) and Cd (Rahman et al., 2016), respectively. Thus, it was observed from the results of this study, that the co-exposure to Cd and aSMPs decreased the physiological toxicity and the stress response of the plants.

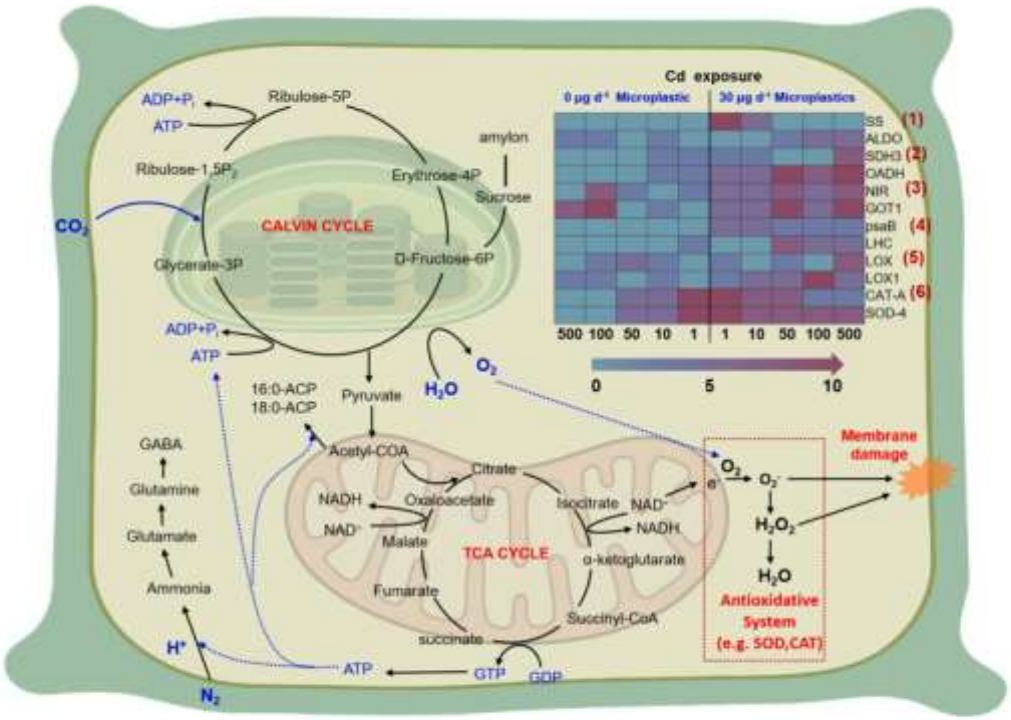

Fig. 5. Integrating omics analysis of joint Cd with aSMPs-Induced stress on rice. Schematic representation of up- or down-regulated pathways after with/without aSMPs application. The inserted heatmaps are related to (1) glycolysis metabolism; (2) TCA cycle; (3) amino acid metabolism; (4) photosynthetic metabolism; (5) fatty acid metabolism; (6) antioxidative system. The Log_2value of gene expression in the heatmaps share the color bar placed at the bottom of heatmap. The ID of genes in heatmaps are described in Table S3.

An extensive set of responses to environmental stress in plants are changes in gene expression. From the aspect of the regulation of more functional differentially expressed genes (DEGs) in plants, the co-exposure group to Cd and aSMPs have less alterations than the individual exposure to Cd (Figure S5 and S7). Previous reports showed that changes in metabolites in rice leaves were induced by the regulation of gene expression. Our results showed that more metabolites alterations in the co-exposure group of Cd and aSMPs than that in the individual Cd exposure (Table S1 and S2). Furthermore, subjected to Cd-induced stress, there was a greater influence on the metabolic pathway of rice leaves in independent Cd exposure groups than the co-exposure groups (Figures S7 and S8). Notably, DEGs were upregulated with increasing Cd levels in co-exposure groups (Figure 5) and were significantly enriched ($p < 0.05$) in the Calvin cycle-related pathway, while in the independent Cd exposure group, it was not up regulated. It could be a defense mechanism in the leaf to maintain physiological homeostasis of the plant (Figure S8A, B).

It was suggested that Cd could affect the expression of genes related to photosynthesis (psbA, psaB, rbcL) and inhibit carbon fixation in plants (Sebastian and Prasad, 2019). Results of our study showed that the changes of psaB (Os07g0148900) were 1.6-fold to 9.4-fold increase in all the co-exposure groups of Cd and aSMPs than that of the independent Cd exposure groups (Figure 5). The reduced carbon fixation efficiency induced by the downregulated Calvin cycle enzymes was probably responsible for the growth inhibition of rice under combined treatments. Several previous studies have also suggested that loss of thylakoid membrane integrity has a direct impact on photosynthetic efficiency (Kusaba et al., 2007). Thylakoids in both co-exposure and independent Cd exposure groups showed a decreasing trend along with the increasement of the exposure concentration. Meanwhile, the slope of decrement was less significant in the co-exposure groups. From the observation of this study, the co-exposure group seems to have a less significant stress to the plant than the independent Cd exposure.

We found that under the stress of the Cd exposure, the light-harvesting capacity of the leaves is affected, which can be attributed to the reduction in the efficiency of the Calvin cycle. Subsequently, the accumulation of sucrose and the downstream starch synthesis are affected by the reduction of photosynthetic products in the

Calvin cycle. Photosynthetic products generate energy (ATP) and electrons by providing the necessary carbon source for the tricarboxylic acid (TCA) cycle. Reducing the efficiency of the Calvin Cycle ultimately leads to reducing the energy and electronic capacity of the TCA Cycle.

At the same time, amino acid, polysaccharide, and protein contents in rice leaves decreased with increasing exposure concentration. Interestingly, in the Cd-exposed group with/without aSMPs, the carbohydrate metabolic pathways (glyoxylate and dicarboxylate metabolism as well as starch and sucrose metabolism) were also declined. This resulted in reduced levels of intermediates such as glucose, maltose (Figure 4). These soluble sugars are critical for plants to maintain turgor pressure and scavenge increased ROS, acting as signals or osmo-protectants in heavy metal-induced pathways (Pidatala et al., 2016).

Our study first time found that compared to the combined Cd and aSMPs exposure group, the independent Cd exposed group showed greater accumulation and toxicity for Cd in rice leaves. A hypothesis has been proposed to explain the results of this study: Aged negatively charged SMPs can capture Cd, thereby reducing Cd exposure in its free state, and jointly inhibit Cd-induced oxidative damage and chloroplast damage, thereby reducing the potential risk of Cd exposure to rice plants.

In this study, there were some limitations that should be mentioned when interpreting the results. First, only the effect of negatively charged aging microplastics in combination with Cd on rice seedlings was considered in the study design, while the effect of aging microplastics with other charges and other stages of the rice life cycle was not investigated. Also, we only considered the scenario where both contaminants were absorbed by the foliage individually and did not include scenarios where one or more of the contaminants were simultaneously exposed to the plant via multiple pathways, such as roots and foliage, respectively. Follow-up studies could also be conducted on the effects of co-exposure to various contaminants over the whole life cycle of rice, providing a basis for a more comprehensive understanding of the ecological risks of aging microplastics and co-exposure to cadmium.

5. Conclusions

The results of this study suggest that Cd accumulation in rice leaves may have a greater environmental and

human health impact than Cd exposure in aSMPs. This is because Cd exposure induced greater physiological, transcriptomic and metabolomic changes in rice leaves, which could have an impact on crop quality and yield. In addition, the study highlights how the abundance and charge properties of SMPs may affect plant growth and physiological metabolism, and how MPs may enter plants through stomatal uptake pathways following foliar exposure. The present study can help to elucidate how Cd and aSMPs affect rice growth and physiological status and provide useful insights into the molecular mechanisms underlying the different biological effects of Cd and aSMPs on rice leaves, which may also be useful in understanding the fate and effects of heavy metal-associated MPs and developing mitigation strategies.

Acknowledgements

This work was jointly supported by the National Natural Science Foundation of China (21906060), Natural Science Foundation of Hubei Province in 2023, the China Postdoctoral Science Foundation (2019M662631, 2021T140235). SY acknowledges FWO junior post-doc fellowships (1270521N). Additionally, we would like to thank the Analytical and Testing Center of Huazhong University of Science and Technology and State key Laboratory of Biogeology and Environmental Geology of China University of Geosciences for providing experimental measurements.

CRediT authorship contribution statement

Xiang Wu: Methodology, Software, Formal analysis, Investigation, Writing - original draft. **Shanshan Yin**: Writing - review & editing. **Yao Liu**: Investigation. **Yuwei Zhu**: Investigation. **Timing Jiang**: Conceptualization, Writing - review & editing. **Sha Liang**: Supervision. **Shijie Bian**: Software, Validation. **Yaowu Cao**: Writing - review & editing. **Guojing Wang**: Data curation. **Jiakuan Yang**: Writing - review & editing.

Appendix A. Supplementary data

The following is the supplementary data to this article:

REFERENCES

Asada, K., 1992. Ascorbate peroxidase – a hydrogen peroxide–scavenging enzyme in plants. ***Physiol Plantarum*** 85(2), 235-241.

Avellan, A., Yun, J., Morais, B., Clement, E., Rodrigues, S., Lowry, G., 2021. Critical review: role of Inorganic Nanoparticle Properties on Their Foliar Uptake and in Planta Translocation. ***Environ Sci Technol*** 55(20), 13417-13431.

Bae, J., Benoit, D., Watson, A., 2016. Effect of heavy metals on seed germination and seedling growth of common ragweed and roadside ground cover legumes. ***Environ Pollut*** 213, 112-118.

Bhagat, K., Barrios, A., Rajwade, K., Kumar, A., Oswald, J., Apul, O., Perreault, F., 2022. Aging of microplastics increases their adsorption affinity towards organic contaminants. ***Chemosphere*** 298, 134238.

Bi, M., He, Q., Chen, Y., 2020. What Roles Are Terrestrial Plants Playing in Global Microplastic Cycling? ***Environ Sci Technol*** 54(9), 5325-5327.

Cai, L., Wang, J., Peng, J., Tan, Z., Zhan, Z., Tan, X., Chen, Q., 2017. Characteristic of microplastics in the atmospheric fallout from Dongguan city, China: preliminary research and first evidence. ***Environ Sci Pollut Res*** 24(32), 24928-24935.

Chiaia-Hernandez, A., Keller, A., Wachter, D., Steinlin, C., Camenzuli, L., Hollender, J., Krauss, M., 2017. Long-Term Persistence of Pesticides and TPs in Archived Agricultural Soil Samples and Comparison with Pesticide Application. ***Environ Sci Technol*** 51(18), 10642-10651.

de Souza Machado, A., Kloas, W., Zarfl, C., Hempel, S., Rillig, M., 2018. Microplastics as an emerging threat to terrestrial ecosystems. ***Glob Chang Biol*** 24(4), 1405-1416.

Ding, L., Mao, R., Ma, S., Guo, X., Zhu, L., 2020. High temperature depended on the ageing mechanism of microplastics under different environmental conditions and its effect on the distribution of organic pollutants. ***Water Res*** 174, 115634.

Dris, R., Gasperi, J., Saad, M., Mirande, C., Tassin, B., 2016. Synthetic fibers in atmospheric fallout: A source of microplastics in the environment? ***Mar Pollut Bull*** 104(1-2), 290-293.

El Rasafi, T., Oukarroum, A., Haddioui, A., Song, H., Kwon, E., Bolan, N., Tack, F., Sebastian, A., Prasad, M., Rinklebe, J., 2020. Cadmium stress in plants: A critical review of the effects, mechanisms, and tolerance strategies. ***Crit Rev Env Sci Tec*** 52(5), 675-726.

Engineer, C., Hashimoto-Sugimoto, M., Negi, J., Israelsson-Nordstrom, M., Azoulay-Shemer, T., Rappel, W., Iba, K., Schroeder, J., 2016. CO_2 Sensing and CO_2 Regulation of Stomatal Conductance: Advances and Open Questions. ***Trends Plant Sci*** 21(1), 16-30.

Green, B., Pichersky, E., Kloppstech, K., 1991. Chlorophyll a/b-binding proteins: an extended family. ***Trends Biochem Sci*** 16(5), 181-186.

Guo, T., Zhang, G., Zhang, Y., 2007. Physiological changes in barley plants under combined toxicity of aluminum, copper and cadmium. ***Colloids Surface B*** 57(2), 182-188.

Gupta, N., Yadav, K., Kumar, V., Kumar, S., Chadd, R., Kumar, A., 2019. Trace elements in soil-vegetables interface: Translocation, bioaccumulation, toxicity and amelioration - A review. ***Sci Total Environ*** 651, 2927-2942.

Hasan, S., Fariduddin, Q., Ali, B., Hayat, S., Ahmad, A., 2009. Cadmium: toxicity and tolerance in plants. ***J Environ Biol*** 30(2), 165-174.

Hong, J., Peralta-Videa, J., Rico, C., Sahi, S., Viveros, M., Bartonjo, J., Zhao, L., Gardea-Torresdey, J., 2014. Evidence of translocation and physiological impacts of foliar applied CeO_2 nanoparticles on cucumber (Cucumis sativus) plants. ***Environ Sci***

Technol 48(8), 4376-4385.

Huang, X., Ming, L., Yang, J., 2015. Effects of coal dust on dust-retention ability and protective enzyme system of leafy vegetables. ***Guangdong Agric. Sci.*** 42, 129-133.

Huffer, T., Metzelder, F., Sigmund, G., Slawek, S., Schmidt, T., Hofmann, T., 2019. Polyethylene microplastics influence the transport of organic contaminants in soil. ***Sci Total Environ*** 657, 242-247.

Jing, H.A., Yang, W.T., Chen, Y.L., Yang, L.Y., Zhou, H., Yang, Y., Zhao, Z.J., Wu, P., Zia-ur-Rehman, M., 2023. Exploring the mechanism of Cd uptake and translocation in rice: Future perspectives of rice safety. ***Sci Total Environ*** 897,165369.

Kalcikova, G., Gotvajn, A., Kladnik, A., Jemec, A., 2017. Impact of polyethylene microbeads on the floating freshwater plant duckweed Lemna minor. ***Environ Pollut*** 230, 1108-1115.

Kusaba, M., Ito, H., Morita, R., Iida, S., Sato, Y., Fujimoto, M., Kawasaki, S., Tanaka, R., Hirochika, H., Nishimura, M., Tanaka, A., 2007. Rice non-yellow coloring1 is involved in light-harvesting complex II and grana degradation during leaf senescence. ***Plant Cell*** 19(4), 1362-1375.

Li, J., Zhang, K., Zhang, H., 2018. Adsorption of antibiotics on microplastics. ***Environ Pollut*** 237, 460-467.

Li, Y., Shao, L., Wang, W., Zhang, M., Feng, X., Li, W., Zhang, D., 2020. Airborne fiber particles: Types, size and concentration observed in Beijing. ***Sci Total Environ*** 705, 135967.

Li, Z., Liang, Y., Hu, H., Shaheen, S., Zhong, H., Tack, F., Wu, M., Li, Y., Gao, Y., Rinklebe, J., Zhao, J., 2021. Speciation, transportation, and pathways of cadmium in soil-rice systems: A review on the environmental implications and remediation approaches for food safety. ***Environ Int*** 156, 106749.

Lian, J., Liu, W., Meng, L., Wu, J., Chao, L., Zeb, A., Sun, Y., 2021. Foliar-applied polystyrene nanoplastics (PSNPs) reduce the growth and nutritional quality of lettuce (Lactuca sativa L.). ***Environ Pollut*** 280, 116978.

Lian, J., Wu, J., Xiong, H., Zeb, A., Yang, T., Su, X., Su, L., Liu, W., 2020a. Impact of polystyrene nanoplastics (PSNPs) on seed germination and seedling growth of wheat (Triticum aestivum L.). ***J Hazard Mater*** 385, 121620.

Lian, J., Wu, J., Zeb, A., Zheng, S., Ma, T., Peng, F., Tang, J., Liu, W., 2020b. Do polystyrene nanoplastics affect the toxicity of cadmium to wheat (Triticum aestivum L.). ***Environ Pollut*** 263, 114498.

Liu, C., Li, J., Zhang, Y., Wang, L., Deng, J., Gao, Y., Yu, L., Zhang, J., Sun, H., 2019. Widespread distribution of PET and PC microplastics in dust in urban China and their estimated human exposure. ***Environ Int*** 128, 116-124.

Liu, J., Zhang, T., Tian, L., Liu, X., Qi, Z., Ma, Y., Ji, R., Chen, W., 2019. Aging Significantly Affects Mobility and Contaminant-Mobilizing Ability of Nanoplastics in Saturated Loamy Sand. ***Environ Sci Technol*** 53(10), 5805-5815.

Liu, K., Wang, X., Fang, T., Xu, P., Zhu, L., Li, D., 2019. Source and potential risk assessment of suspended atmospheric microplastics in Shanghai. ***Sci Total Environ*** 675, 462-471.

Liu, K., Wang, X., Song, Z., Wei, N., Li, D., 2020. Terrestrial plants as a potential temporary sink of atmospheric microplastics during transport. ***Sci Total Environ*** 742, 140523.

Liu, P., Qian, L., Wang, H.Y., Zhan, X., Lu, K., Gu, C., Gao, S.X., 2019. New Insights into the Aging Behavior of Microplastics Accelerated by Advanced Oxidation Processes. ***Environ Sci Technol*** 53(7), 3579-3588.

Liu, W., Zhou, Q., An, J., Sun, Y., Liu, R., 2010. Variations in cadmium accumulation among Chinese cabbage cultivars and screening for Cd-safe cultivars. ***J Hazard Mater*** 173(1-3), 737-743.

Liu, Y., Wu, T., White, J., Lin, D., 2021. A new strategy using nanoscale zero-valent iron to simultaneously promote remediation and safe crop production in contaminated soil. ***Nat Nanotechnol*** 16(2), 197-205.

Lu, H., Zhang, Y., Wu, Y., 2020. Research progress on foliar absorption mechanism of pollutants. ***Huanjing Huaxue-Environmental Chemistry*** 39(12), 3371-3383.

Lu, Q., Zhou, Y., Sui, Q., Zhou, Y., 2023. Mechanism and characterization of microplastic aging process: A review. ***Front Environ Sci Eng*** 17(8),100.

Lv, J., Christie, P., Zhang, S., 2019. Uptake, translocation, and transformation of metal-based nanoparticles in plants: recent advances and methodological challenges. ***Environ Sci: Nano*** 6(1), 41-59.

Nikolić, N., Pajević, S., Župunski, M., Topić, M., Arsenov, D., 2014. Responses of Wheat (Triticum Aestivum L.) and Maize (Zea Mays L.) Plants to Cadmium Toxicity in Relation to Magnesium Nutrition. ***Acta Botanica Croatica*** 73(2), 359-373.

Ouyang, X., Ma, J., Liu, Y., Li, P., Wei, R., Chen, Q., Weng, L., Chen, Y., Li, Y., 2023. Foliar cadmium uptake, transfer, and redistribution in Chili: A comparison of foliar and root uptake, metabolomic, and contribution. ***J Hazard Mater*** 453, 131421.

Pang, Z., Zhou, G., Ewald, J., Chang, L., Hacariz, O., Basu, N., Xia, J., 2022. Using MetaboAnalyst 5.0 for LC-HRMS spectra processing, multi-omics integration and covariate adjustment of global metabolomics data. ***Nature Protocols*** 17(8), 1735-1761.

Perez-Romero, J., Redondo-Gomez, S., Mateos-Naranjo, E., 2016. Growth and photosynthetic limitation analysis of the Cd-accumulator Salicornia ramosissima under excessive cadmium concentrations and optimum salinity conditions. ***Plant Physiol Bioch*** 109, 103-113.

Pidatala, V., Li, K., Sarkar, D., Ramakrishna, W., Datta, R., 2016. Identification of Biochemical Pathways Associated with Lead Tolerance and Detoxification in Chrysopogon zizanioides L. Nash (Vetiver) by Metabolic Profiling. ***Environ Sci Technol*** 50(5), 2530-2537.

Rahman, A., Nahar, K., Hasanuzzaman, M., Fujita, M., 2016. Manganese-induced cadmium stress tolerance in rice seedlings: Coordinated action of antioxidant defense, glyoxalase system and nutrient homeostasis. ***C R Biol*** 339(11-12), 462-474.

Rellan-Alvarez, R., Ortega-Villasante, C., Alvarez-Fernandez, A., del Campo, F., Hernandez, L., 2006. Stress responses of Zea mays to cadmium and mercury. ***Plant and Soil*** 279(1-2), 41-50.

Revell, L., Kuma, P., Le Ru, E., Somerville, W., Gaw, S., 2021. Direct radiative effects of airborne microplastics. ***Nature*** 598(7881), 462-467.

Rizwan, M., Ali, S., Rehman, M., Rinklebe, J., Tsang, D., Bashir, A., Maqbool, A., Tack, F., Ok, Y., 2018. Cadmium phytoremediation potential of Brassica crop species: A review. ***Sci Total Environ*** 631-632, 1175-1191.

Saleh, S., Kandeel, M., Ghareeb, D., Ghoneim, T., Talha, N., Alaoui-Sosse, B., Aleya, L., Abdel-Daim, M., 2020. Wheat biological responses to stress caused by cadmium, nickel and lead. ***Sci Total Environ*** 706, 136013.

Sebastian, A., Prasad, M., 2019. Photosynthetic light reactions in Oryza sativa L. under Cd stress: Influence of iron, calcium, and zinc supplements. ***Eurobiotech J*** 3(4), 175-181.

Sengupta, A., Webb, R., Holaday, A., Allen, R., 1993. Overexpression of Superoxide Dismutase Protects Plants from Oxidative Stress (Induction of Ascorbate Peroxidase in Superoxide Dismutase-Overexpressing Plants). ***Plant Physiol*** 103(4), 1067-1073.

Shaw, A., Hossain, Z., 2013. Impact of nano-CuO stress on rice (Oryza sativa L.) seedlings. ***Chemosphere*** 93(6), 906-915.

Soudek, P., Petrova, S., Vankova, R., Song, J., Vanek, T., 2014. Accumulation of heavy metals using Sorghum sp. ***Chemosphere*** 104, 15-24.

Sun, J., Pan, L., Tsang, D., Zhan, Y., Zhu, L., Li, X., 2018. Organic contamination and remediation in the agricultural soils of China: A critical review. ***Sci Total Environ*** 615, 724-740.

Tang, F., Lenzen, M., McBratney, A., Maggi, F., 2021. Risk of pesticide pollution at the global scale. ***Nature Geoscience*** 14(4),

206-210.

Vassilev, A., Lidon, F., Matos, M., Ramalho, J., Yordanov, I., 2002. Photosynthetic Performance and Content of Some Nutrients in Cadmium- and Copper-Treated Barley Plants. ***Journal of Plant Nutrition*** 25(11), 2343-2360.

Velzeboer, I., Kwadijk, C., Koelmans, A., 2014. Strong sorption of PCBs to nanoplastics, microplastics, carbon nanotubes, and fullerenes. ***Environ Sci Technol*** 48(9), 4869-4876.

Wang, J., Zhang, X.K., Li, X.A., Wang, Z.Y., 2023. Exposure pathways, environmental processes and risks of micro (nano) plastics to crops and feasible control strategies in agricultural regions. ***J Hazard Mater*** 459,132269.

Wang, Y., Wang, F., Xiang, L., Bian, Y., Wang, Z., Srivastava, P., Jiang, X., Xing, B., 2022a. Attachment of positively and negatively charged submicron polystyrene plastics on nine typical soils. ***J Hazard Mater*** 431, 128566.

Wang, Y., Xiang, L., Wang, F., Wang, Z., Bian, Y., Gu, C., Wen, X., Kengara, F., Schaeffer, A., Jiang, X., Xing, B., 2022b. Positively Charged Microplastics Induce Strong Lettuce Stress Responses from Physiological, Transcriptomic, and Metabolomic Perspectives. ***Environ Sci Technol*** 56(23), 16907-16918.

Wang, Y., Xiang, L.L., Wang, F., Redmile-Gordon, M., Bian, Y.R., Wang, Z.Q., Gu, C.G., Jiang, X., Schäffer, A., Xing, B.S., 2023. Transcriptomic and metabolomic changes in lettuce triggered by microplastics-stress. ***Environ Pollut*** 320, 121081.

Willekens, H., Chamnongpol, S., Davey, M., Schraudner, M., Langebartels, C., VanMontagu, M., Inze, D., VanCamp, W., 1997. Catalase is a sink for H2O2 and is indispensable for stress defence in C-3 plants. ***Embo Journal*** 16(16), 4806-4816.

Wu, X., Hou, H., Liu, Y., Yin, S., Bian, S., Liang, S., Wan, C., Yuan, S., Xiao, K., Liu, B., Hu, J., Yang, J., 2022. Microplastics affect rice (Oryza sativa L.) quality by interfering metabolite accumulation and energy expenditure pathways: A field study. ***J Hazard Mater*** 422, 126834.

Wu, X., Liu, Y., Yin, S., Xiao, K., Xiong, Q., Bian, S., Liang, S., Hou, H., Hu, J., Yang, J., 2020. Metabolomics revealing the response of rice (Oryza sativa L.) exposed to polystyrene microplastics. ***Environ Pollut*** 266, 115159.

Xiong, T., Dumat, C., Dappe, V., Vezin, H., Schreck, E., Shahid, M., Pierart, A., Sobanska, S., 2017. Copper Oxide Nanoparticle Foliar Uptake, Phytotoxicity, and Consequences for Sustainable Urban Agriculture. ***Environ Sci Technol*** 51(9), 5242-5251.

Xiong, T., Zhang, S., Kang, Z., Zhang, T., Li, S., 2021. Dose-Dependent Physiological and Transcriptomic Responses of Lettuce (Lactuca sativa L.) to Copper Oxide Nanoparticles-Insights into the Phytotoxicity Mechanisms. ***Int J Mol Sci*** 22(7), 26.

Xu, C.Y., Zhang, B.B., Gu, C.J., Shen, C.S., Yin, S.S., Aamir, M., Li, F., 2020. Are we underestimating the sources of microplastic pollution in terrestrial environment? ***J Hazard Mater*** 400,123228.

Young, A., 1991. The photoprotective role of carotenoids in higher plants ***Physiol Plantarum*** 83(4), 702-708.

Zeb, A., Liu, W., Meng, L., Lian, J., Wang, Q., Lian, Y., Chen, C., Wu, J., 2022. Effects of polyester microfibers (PMFs) and cadmium on lettuce (Lactuca sativa) and the rhizospheric microbial communities: A study involving physio-biochemical properties and metabolomic profiles. ***J Hazard Mater*** 424, 127405.

Zhang, K., Hamidian, A., Tubic, A., Zhang, Y., Fang, J., Wu, C., Lam, P., 2021. Understanding plastic degradation and microplastic formation in the environment: A review. ***Environ Pollut*** 274, 116554.

Zhang, M., Liu, Z., Zhou, C., 2010. Effect of atmospheric deposition on heavy metal accumulation in vegetable crop near a lead-zinc smelt mine. ***Journal of Zhejiang University (Agriculture and Life Sciences)*** 36(2), 221-229.

Zhang, Y., Gao, T., Kang, S., Sillanpaa, M., 2019. Importance of atmospheric transport for microplastics deposited in remote areas. ***Environ Pollut*** 254, 112953.

Zhao, J., Ren, W., Dai, Y., Liu, L., Wang, Z., Yu, X., Zhang, J., Wang, X., Xing, B., 2017. Uptake, Distribution, and

Transformation of CuO NPs in a Floating Plant Eichhornia crassipes and Related Stomatal Responses. ***Environ Sci Technol*** 51(13), 7686-7695.

Zhou, C., Lu, C., Mai, L., Bao, L., Liu, L., Zeng, E., 2021. Response of rice (Oryza sativa L.) roots to nanoplastic treatment at seedling stage. ***J Hazard Mater*** 401, 123412.

Zouari, M., Ben Ahmed, C., Elloumi, N., Bellassoued, K., Delmail, D., Labrousse, P., Ben Abdallah, F., Ben Rouina, B., 2016. Impact of proline application on cadmium accumulation, mineral nutrition and enzymatic antioxidant defense system of Olea europaea L. cv Chemlali exposed to cadmium stress. ***Ecotox Environ Safe*** 128, 195-205.

Supplementary Information

Molecular Mechanisms and Physiological Responses of Rice Leaves co-exposed to Submicron-Plastics and Cadmium: Implication for Food Quality and Security

Xiang Wu [a, b], Shanshan Yin[e], Yao Liu[f], Yuwei Zhu[a, c], Timing Jiang[a, c], Sha Liang[a, c], Shijie Bian[a, c], Yaowu Cao[b], Guojing Wang[b], Jiakuan Yang[*, a, c, d]

a *School of Environmental Science & Engineering, Huazhong University of Science & Technology, Wuhan, Hubei, 430074, China*

b *School of Resources and Environmental Science, Hubei University, Wuhan 430062, China*

c *Hubei Provincial Engineering Laboratory of Solid Waste Treatment, Disposal and Recycling, Wuhan, Hubei, 430074, China*

d State Key Laboratory of Coal Combustion, Huazhong University of Science & Technology, Wuhan, Hubei, 430074, China

e *Toxicological Center, Universiteit Antwerpen, Universiteitsplein 1, Wilrijk 2610, Belgium*

f College of Environmental and Biological Engineering, Wuhan Technology and Business University, Wuhan, Hubei, 430065, China

[*] **Corresponding author:** Prof. Jiakuan Yang

Email addresses: jkyang@mail.hust.edu.cn; yjiakuan@hotmail.com

Tel: +86-27-87540995; Fax: +86-27-87792207

This material contains 48 pages, 7 texts, 9 figures, and 4 tables.

Contents

Text S1. Preparation of aSMPs suspensions

Microplastics have similar properties to those of nanoparticles. A large amount of positive and negative charges are accumulated on the surface when the particle of microplastics are refined to the nano- level, which would cause accumulation of charge. The microplastic particles have a large surface area, resulting in highly chemically active and exhibiting strong surface effects of particles. These properties cause the microplastics to accumulate and reach a stable state. The main cause of particle agglomeration in liquid media is the result of a combination of adsorption and repulsion. The agglomeration of the microplastic particles is difficult to disperse using an ultrasonic wave, and thus a method of dispersing the microplastic particles was approached.

Polyvinyl pyrrolidone K-30 (PVP) was added to a certain amount of ultrapure water. Then n-dodecyl β-D-maltoside, 4-(2-Hydroxyethyl)-1-piperazineethanesulfonic acid (HEPES), potassium chloride, magnesium chloride, and sodium chloride were also added. The solution was tolerance to 1L after complete dissolution. In this suspension solution, PVP, n-Dodecyl β-D-maltoside and HEPES act as a stabilizer, a nonionic biosurfactant, and an ionic buffer, respectively. Potassium chloride, sodium chloride, and magnesium chloride provide the appropriate ionic strength to the solution. The microplastic was uniformly dispersed in 50 ml of the PVP suspension solution and then this suspension solution was added to the hydroponic nutrient solution or field soil. Concentrations of other ions (PVP, n-Dodecyl β-D-maltoside and HEPES) in the MP suspension mother liquor do not exceed 1%, so it was assumed that other ions in the suspensions would not affect experimental results.

Text S2. LA-ICP-MS measurements.

LA-ICP-MS measurements were performed on an ArF excimer 193 nm laser ablation system with a standard ablation cell coupled to a quadrupole ICP-MS (Agilent 7700x, Agilent Technologies, Inc., USA) instrument. Samples were quantified using internal standard method, with a calibration was done by spiking Cd standards into blank rice leave samples, and the $r^2 > 0.999$.

For QC of the analysis, a silicate glass reference material (NIST SRM 610) was used for routine tuning

to obtain the maximum signal intensity of $^{238}U^{+}$, to maintain a $^{238}U^{+}/^{232}Th^{+}$ ratio close to 1, and to ensure low oxide formation ($^{232}Th^{16}O^{+}/^{232}Th^{+}$ < 0.5%). Two approaches were used to reduce the possible effects of humidity in the LA-ICP-MS analysis, namely, (1) real-time monitoring of the room temperature at 22 °C and 40%, and (2) all solid pellets (standards or samples) were preserved in a dryer before and after sample analysis.

Data processing, off-line selection, and integration of the background and the analyte signals were performed using ICP-MS Data Cal software.

LA-ICP-MS operating conditions [1]

Laser ablation system	ArF excimer nanosecond laser
Wavelength, nm	193
Energy density, J cm^{-2}	7
Repetition rate, Hz	10
Spot size, μm	90
Line scan speed, μm s^{-1}	15
Carrier gas (He) flow rate, L min^{-1}	0.80

ICP-MS system	Agilent 7700x
RF power, W	1550
Auxiliary gas (Ar) flow rate, L min^{-1}	0.85
Plasma gas (Ar) flow rate, L min^{-1}	15
Dwell time per isotope, ms	10
Monitored isotopes (LOD, μg g^{-1})	^{113}Cd

Text S3. Methods of polysaccharide, protein, and free amino acids content of leaves

Polysaccharide Content. Soluble sugars in grains were extracted and quantified by a modified version of the method reported by Du et al. [2] About 0.1 g of the fresh ground sample was extracted with 2 mL of 80% (v/v) ethanol at 80 °C for 30 min, followed by centrifugation at 3000 *g* for 10 min, with the process then repeated two more times. Then, the supernatants were combined for the measurement of the soluble sugar content. Furthermore, the residues were evaporated to remove ethanol and then

successively hydrolyzed in 9.2 and 4.6 mol/L perchloric acid. After centrifugation at 3000 *g*, the perchloric acid supernatants were collected for measurement of the starch contents. Finally, the determination of starch and soluble sugar concentrations was performed using the anthrone methods.[3]

Protein and Free Amino Acids Content. The nitrogen content was determined by an automated analysis system K1100 (Haineng, China). The protein contents were calculated by a protein-to-nitrogen conversion factor of 5.95 according to the methods reported by Bagchi et al. [4] 0.1 g of fresh grains ground in liquid nitrogen was hydrolyzed in 5 mL of 3% (w/v) of sulfosalicylic acid for 1 h and then centrifuged at 10,000 *g* for 15 min. The supernatant was filtered through a 0.22 μm filter membrane for the quantification of amino acids using an automatic amino acid analyzer S-433D (Sykam, German).

Text S4. Oxidative Damage and Antioxidant Enzyme Activities Assay

The 0.1 g of fresh leaves were ground with liquid nitrogen, and then added 8 mL of 0.05 M Na_2HPO_4/NaH_2PO_4 (pH 7.8) buffer. The homogenates were collected and centrifuged at 4 °C for 15 min at 10 000g. The supernatants were collected as crude enzyme.

Activity of CAT was measured by the decomposition rate of H_2O_2 at 240 nm. For POD, the activity was measured by the oxidation rate of guaiacol at 470 nm. Activities for CAT and POD were expressed in enzyme units/mg (U/mg) FW, where one enzyme unit was defined as a change of 0.01 absorbance per min caused by the enzyme aliquot. The activity of SOD was defined by the amount of enzyme causing 50% inhibition of NBT reduction at 560 nm.[5,6]

The MDA amount was calculated using the absorbance of the supernatant at 532 nm subtracting the non-specific absorbance at 600 nm and 450 nm, after 5 mL of homogenates was boiled for 10 min with 5 mL 0.5% trichloroacetic acid solution.

Text S5. Method of metabolites extraction and derivatization

Metabolites Extraction. Specifically, a total of 0.1 g of rice samples ground with zirconium beads were weighed and then extracted with 1.4 mL of a chloroform: water: methanol (2:2:5, v/v/v, stored at 4 °C)

mixture consisting of 0.2 mg mL^{-1} ribitol (internal standard) for 1 h at 4 °C. Following centrifugation at 10,000 *g* for 10 min, 400 µL of the supernatant was collected and freeze dried for derivatization (60 µL of 20 mg mL^{-1} O-methoxyamine hydrochloride in pyridine at 37 °C for 90 min then 80 µL of MSTFA at 37 °C for 30 min) before analysis by instruments.[7]

Metabolites Detection. After metabolites extraction, Derivative samples (1 µL) were immediately determined using a gas chromatography system (GC, Agilent 7890B, USA) coupled with a quadrupole mass spectrometry (MS, Agilent 5977B, USA). The sample was injected into the GC column (DB-5MS fused-silica capillary column, 30 m × 0.25 mm × 0.25 µm; Agilent J & W Scientific, Folsom, CA, USA Agilent Technologies, Santa Clara, CA) in a split mode (1:15). Helium (>99.999%) was maintained at a constant flow rate of 1.0 mL $^{-1}$min as the carrier gas. The injection port, the transfer line, and ion source temperatures were held at 260, 280, and 230 °C. The initial oven temperature was 60 °C, ramped to 125 °C at a rate of 8 °C/min, to 210 °C at a rate of 4 °C/min, to 270 °C at a rate of 5 °C/min, to 305 °C at a rate of 10 °C/min, and finally, held at 305 °C for 3 min. The solvent delay was set at 5 min. The electron energy of electron impact ionization (EI^+) was set as 70 eV. Mass spectra were acquired using full scan monitoring mode, and the mass scan range was from m/z 30 to 600. The quality control samples were injected at regular intervals (every 5 samples).

Text S6. Transcriptome Analysis

RNA-Seq was performed at Novogene Biotech Co., Ltd. (Beijing, China) based on the manufacturer's instructions.

RNA Extraction. Total RNA was extracted from fresh grain tissues using the RNeasy mini kit (QIAGEN, Germantown, MD, USA) based on the manufacturer's instructions. Genomic DNA was removed using DNase I (Takara). Then RNA quality was determined by 2100 Bioanalyser (Agilent Technologies) and quantified using the NanoPhotometer® spectrophotometer (IMPLEN, CA, USA). Only a high-quality RNA sample (OD260/280=1.8~2.2, OD260/230≥2.0, RIN≥6.5, 28S:18S≥1.0, >2 µg) was used to construct a sequencing library.

Library preparation for Transcriptome sequencing. 1 μg of total RNA per sample was used as input material for the RNA sample preparations. Sequencing libraries were generated using NEBNext® UltraTM RNA Library Prep Kit for Illumina® (NEB, USA) following the manufacturer's recommendations and index codes were added to attribute sequences to each sample. Briefly, mRNA was purified from total RNA using poly-T oligo-attached magnetic beads. Fragmentation was carried out using divalent cations under elevated temperature in NEBNext First Strand Synthesis Reaction Buffer (5X). First-strand cDNA was synthesized using random hexamer primer and M-MuLV Reverse Transcriptase (RNase H-). Second strand cDNA synthesis was subsequently performed using DNA Polymerase I and RNase H. Remaining overhangs were converted into blunt ends via exonuclease/polymerase activities. After adenylation of 3' ends of DNA fragments, NEBNext Adaptor with hairpin loop structure was ligated to prepare for hybridization. To select cDNA fragments of preferentially 250-300 bp in length, the library fragments were purified with the AMPure XP system (Beckman Coulter, Beverly, USA). Then 3 μL USER Enzyme (NEB, USA) was used with the size selected, adaptor-ligated cDNA at 37 °C for 15 min followed by 5 min at 95 °C before PCR. Then PCR was performed with Phusion High-Fidelity DNA polymerase, Universal PCR primers, and Index (X) Primer. At last, PCR products were purified (AMPure XP system) and library quality was assessed on the Agilent Bioanalyzer 2100 system. The clustering of the index-coded samples was performed on a cBot Cluster Generation System using TruSeq PE Cluster Kit v3-cBot-HS (Illumia) according to the manufacturer's instructions. After cluster generation, the library preparations were sequenced on an Illumina Novaseq platform and 150 bp paired-end reads were generated.

Reads mapping. The raw paired-end reads were trimmed, and quality controlled by SeqPrep (https://github.com/jstjohn/SeqPrep) and Sickle (https://github.com/najoshi/sickle) with default parameters. Then clean reads were separately aligned to reference genome with orientation mode using TopHat (http://tophat.cbcb.umd.edu/version 2.1.1) software.[8] The mapping criteria of bowtie were as follows: sequencing reads should be uniquely matched to the genome allowing up to 2 mismatches,

without insertions or deletions. After then, the gene region was expanded following depths of sites and the operon was acquired. In addition, the whole genome was split into multiple 15 kb windows that share 5 kb. New transcribed regions were defined as above 2 consecutive windows without overlapped gene region, where at least 2 reads mapped per window in the same orientation. Reference genome and gene model annotation files were downloaded from the genome website directly. Index of the reference genome was built and paired-end clean reads were aligned to the reference genome using Hisat2 v2.0.5. We selected Hisat2 as the mapping tool for that Hisat2 can generate a database of splice junctions based on the gene model annotation file, thus obtaining a better mapping result compared to other non-splice mapping tools.

Differential expression analysis and Functional Enrichment. Differential expression analysis of two conditions/groups (three biological replicates per condition) was performed using the DESeq2 R package (1.16.1). DESeq2 provides statistical routines for determining differential expression in digital gene expression data using a model based on the negative binomial distribution. The resulting *P*-values were adjusted using Benjamini and Hochberg's approach for controlling the false discovery rate. Genes with an adjusted *P*-value <0.05 found by DESeq2 were assigned as differentially expressed. featureCounts v1.5.0-p3 was used to count the reads numbers mapped to each gene. And then fragments per kilobase of exon model per million mapped fragments (FPKM) of each gene was calculated based on the length of the gene and reads count mapped to this gene. FPKM, the expected number of Fragments Per Kilobase of transcript sequence per Millions of base pairs sequenced, considers the effect of sequencing depth and gene length for the reads count at the same time, and is currently the most used method for estimating gene expression levels.

Gene Ontology (GO) enrichment analysis of differentially expressed genes was implemented by the cluster profile R package, in which gene length bias was corrected.

GO terms with corrected *P*-value less than 0.05 were considered significantly enriched by differential expressed genes. KEGG is a database resource for understanding high-level functions and utilities of

the biological system, such as the cell, the organism, and the ecosystem, from molecular-level information, especially large-scale molecular datasets generated by genome sequencing and other high-throughput experimental technologies (http://www.genome.jp/kegg/). We used the cluster profile R package to test the statistical enrichment of differential expression genes in KEGG pathways.

***Gene Set Enrichment Analysis*.** Gene Set Enrichment Analysis (GSEA) is a computational approach to determine if a pre-defined Gene Set can show a significant consistent difference between two biological states. The genes were ranked according to the degree of differential expression in the two samples, and then the predefined Gene Set was tested to see if they were enriched at the top or bottom of the list. Gene set enrichment analysis can include subtle expression changes. We use the local version of the GSEA analysis tool http://www.broadinstitute.org/gsea/index.jsp. GO, KEGG, Reactome, DO, DisGeNET data set were used for GSEA independently.

Text S7. Substructure detection by Transmission Electron Microscopy.

Rice leaves in all groups were cut to 1 cm^2 pieces and fixed for over 12 h in a 0.1 mol L^{-1} cacodylate buffer solution containing 2.5% glutaraldehyde (pH7.4), with all samples taken from the same position on leaves.

Then, the collected sample pieces were treated with 1.0% OsO_4 for 1.5 h and dehydrated in ethanol for five times. Following this, samples were embedded in epoxy resin and ultrathin sections (70–90 nm) were obtained using a Reichert Ultra cuts ultramicrotome (Tokyo, Japan), and stained with uranyl acetate by lead citrate. Finally, all samples were observed with a JEM-1230 microscope (JEOL Ltd., Tokyo, Japan

References：

1. Zhou, J.; Guo, W.; Jin, L.; Hu, S., Elemental Analysis of Solid Food Materials Using a Reliable Laser Ablation Inductively Coupled Plasma Mass Spectrometry Method. ***J. Agric. Food Chem.*** 2022, 70, (15), 4765-4773.
2. Du, Y.; Zhao, Q.; Chen, L.; Yao, X.; Zhang, W.; Zhang, B.; Xie, F., Effect of drought stress on sugar metabolism in leaves and roots of soybean seedlings. ***Plant Physiol. Biochem.*** 2020, 146, 1-

12.

3. Liu, N.; Zhu, L., Metabolomic and transcriptomic investigation of metabolic perturbations in Oryza sativa L. triggered by three pesticides. ***Environ. Sci. Technol.*** 2020, 54, (10), 6115-6124.
4. T. Bagchi.; S. Sharma.; K. Chattopadhyay, Development of NIRS models to predict protein and amylose content of brown rice and proximate compositions of rice bran. ***Food Chem.*** 2016, 191, 21-27.
5. Dewey, C. N.; Li, B. RSEM: accurate transcript quantification from RNA-Seqdata with or without a reference genome. ***BMC Bioinformatics*** 2011, 12, (1),323−323.
6. Robinson, M. D.; Mccarthy, D. J.; Smyth, G. K. edge R: a Bioconductor package for differential expression analysis of digital gene expression data. ***Bioinformatics*** 2010, 26, (1), 139-140.
7. Zhang, L.; Wang, X.; Guo, J.; Xia, Q.; Zhao, G.; Zhou, H.; Xie, F. Metabolic profiling of Chinese tobacco leaf of different geographical origins by GC-MS. ***J. Agric. Food Chem.*** 2013, 61, 2597-2605.
8. Trapnell, C.; Pachter, L.; Salzberg, S. L. TopHat: discovering splice junctions with RNA-Seq. ***Bioinformatics***.2009, 25, (9), 1105−1111.

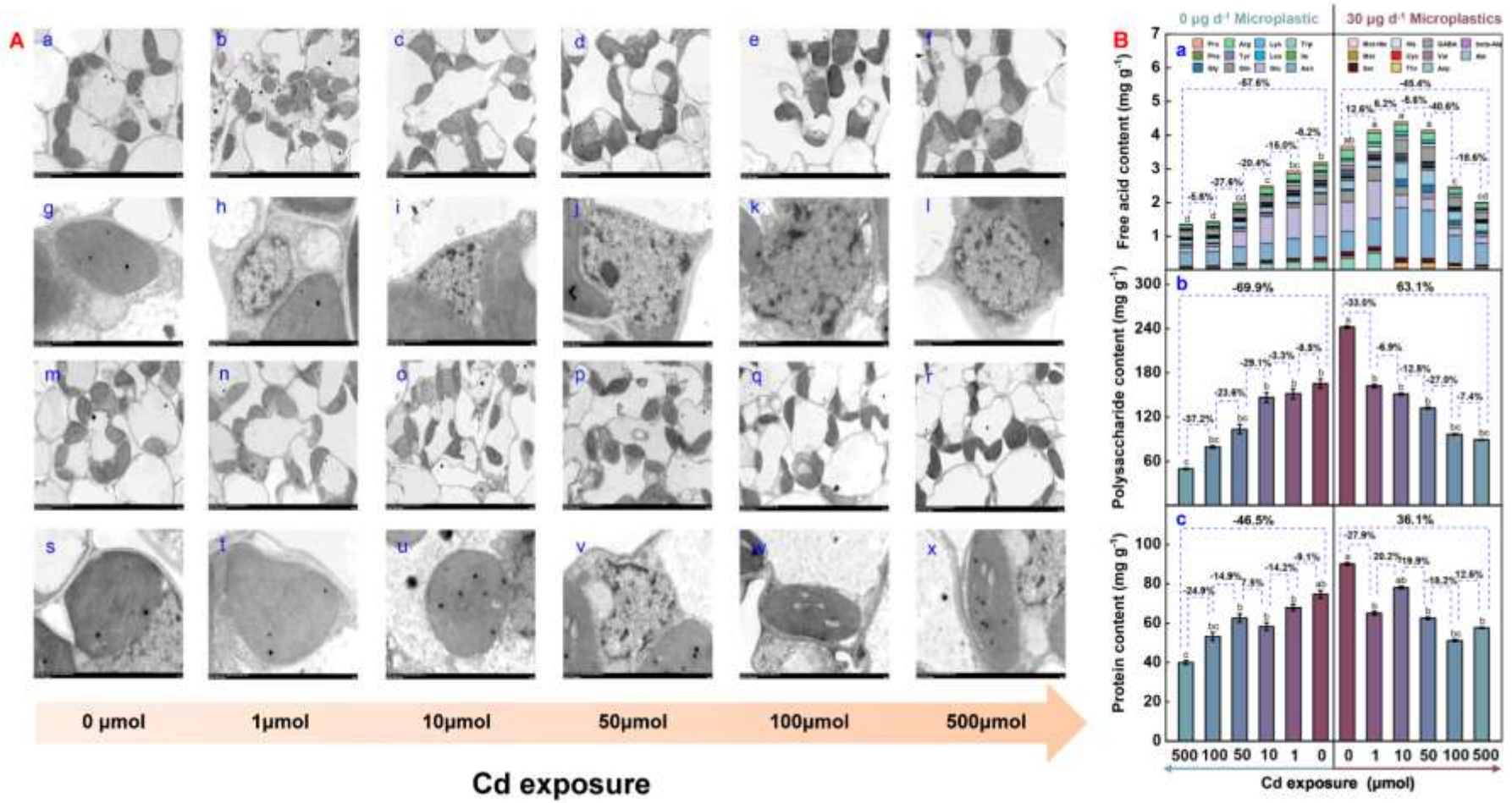

Figure S1. Transmission Electron Microscope (TEM) images (A, a−x) and polysaccharide, protein, and free amino acids content of leaves (B, a-c). A(a-i) are the TEM image under 0, 1, 10, 50, 100 and 500 µmol Cd exposure with 0 µg d^{-1} microplastic and (m-x) are the TEM image under 0,

1, 10, 50, 100 and 500 μmol Cd exposure with 30 μg d^{-1} aSMPs. g, h, i, j, k and s, t, u, v, w, x are enlargements of the areas of nucleus in a, b, c, d, e, f and m, n, o, p, q, r, respectively. Free amino acids (B, a), Polysaccharide (B, b) and protein (B, c) content of leaves following foliar exposure to differentially charged Cd with/without aSMPs. Different lowercase letters indicate significant differences between the different treatments ($p < 0.05$). The percentage figures show the magnitude of change between the different treatment groups (0/1μM, 1/10μM, 10/100μM, 100/500μM and 0/500μM, with/without aSMPs).

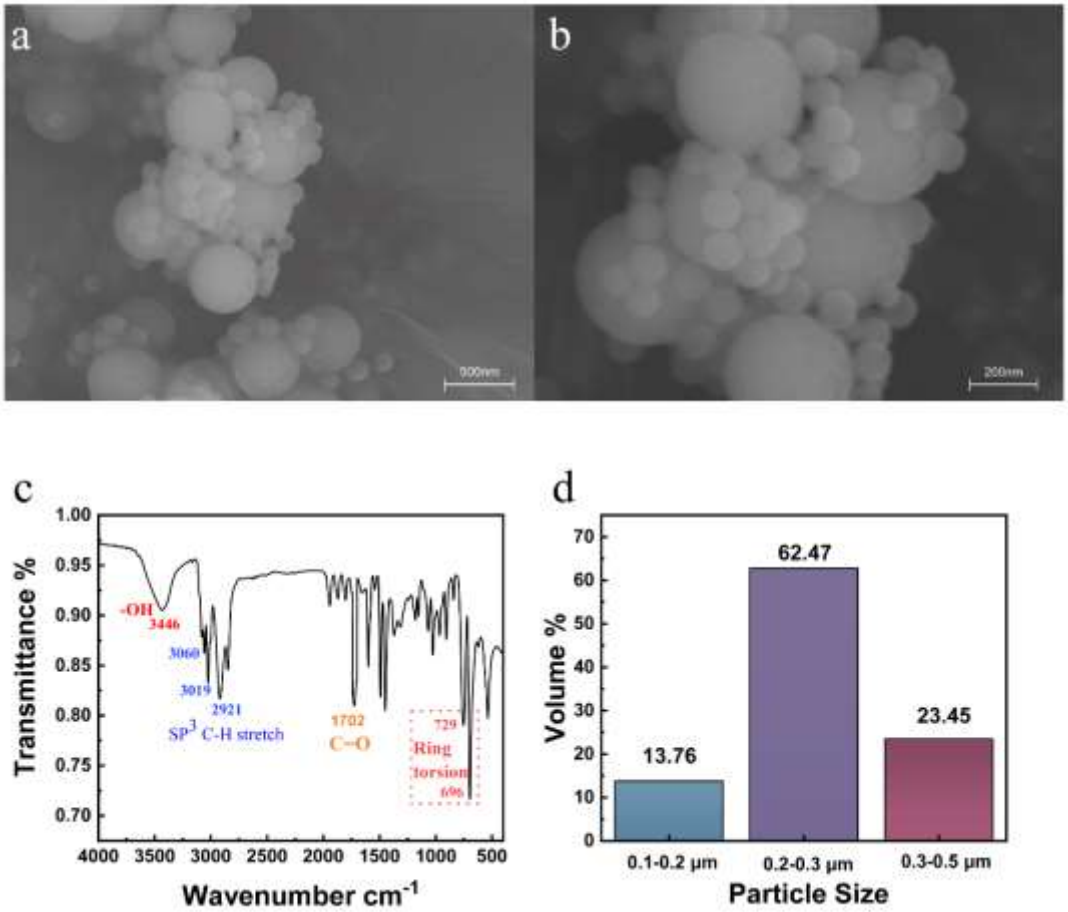

Figure S2. Characteristics of the aged Submicron-plastics (aSMPs): (a) SEM image with low magnification; (b) SEM image with high magnification; (c) FTIR spectra of the aSMPs; (d) Particle size distribution according to Dynamic Light Scattering in deionized water.

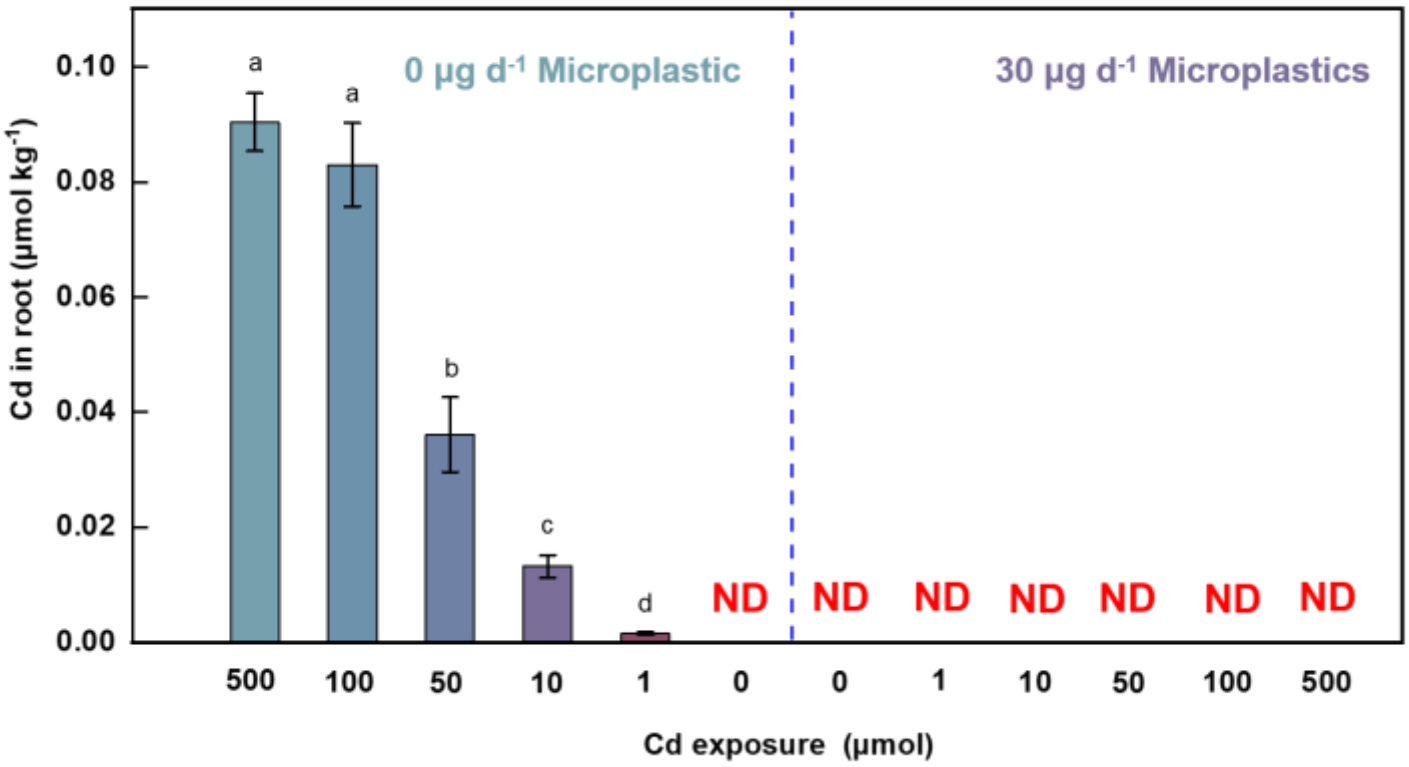

Figure S3. Quantification of Cd in rice root by ICP-MS. Foliar spray of 0, 1, 10, 50, 100 and 500 μM Cd exposure combined 0 μg d^{-1} microplastic and 30 μg d^{-1} SMPs.

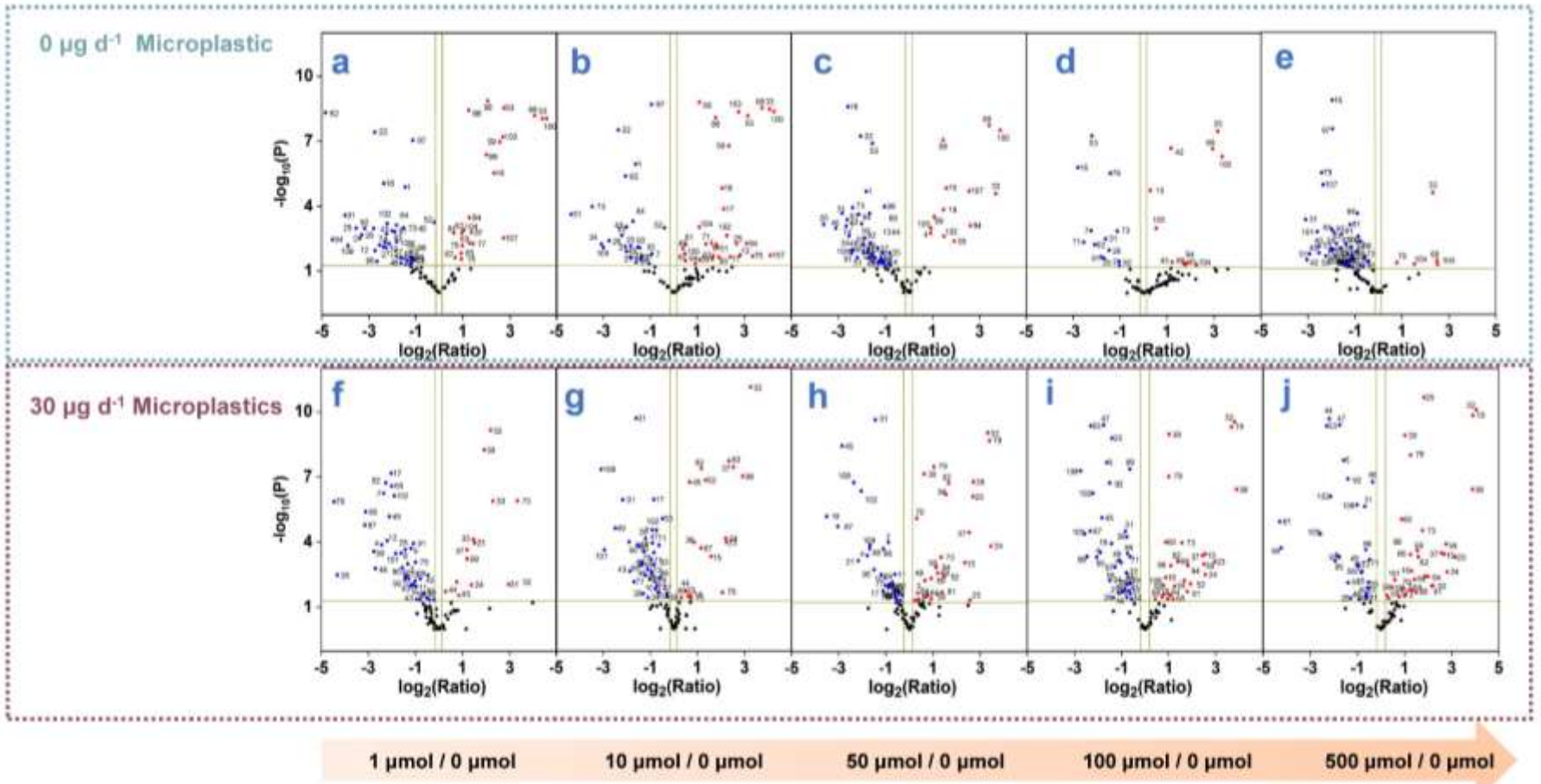

Figure S4. The volcano plots of differentially metabolites group (1/0μM, 10/0μM, 50/0μM, 100/0μM and 500/0μM) exposed to 0 μg d^{-1} microplastic and 30 μg d^{-1} aSMPs. Full metabolite names are provided in Tables S1 and S2. Red and blue indicate up-and down-regulation of metabolites.

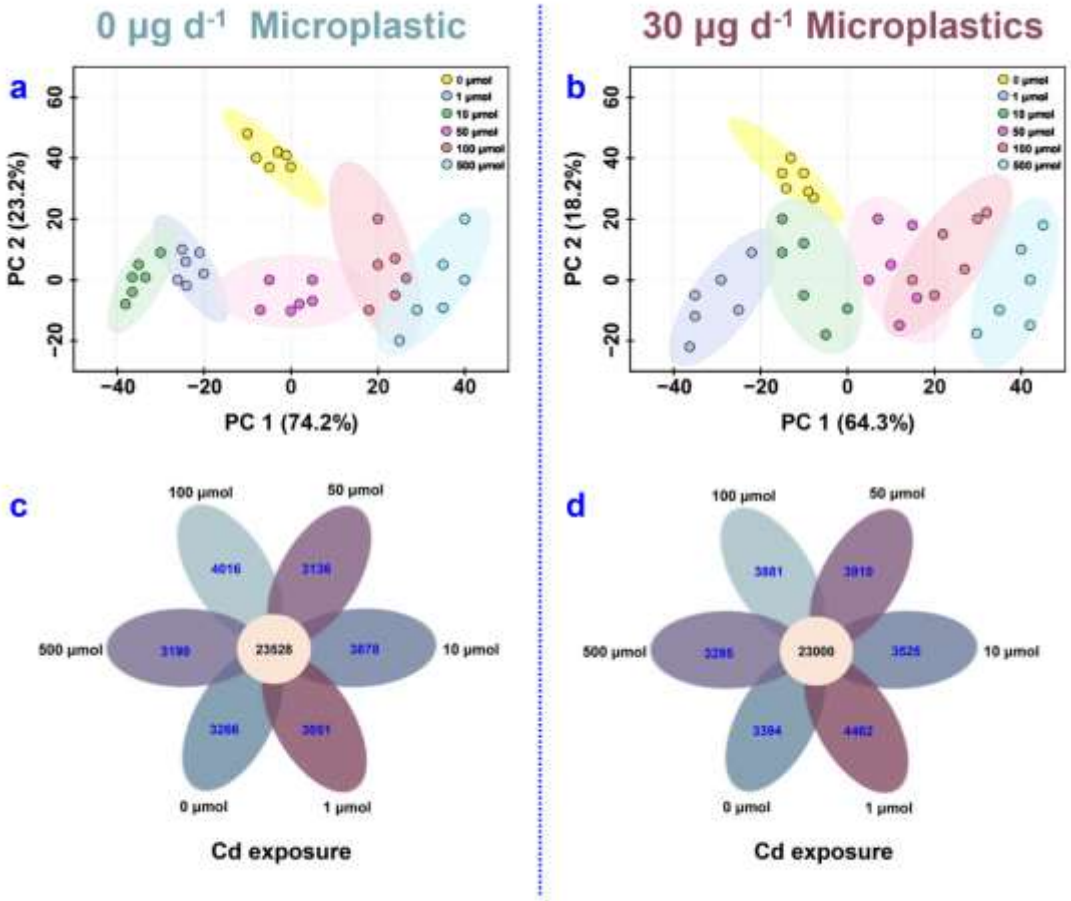

Figure S5. Sample variance analysis of differentially expressed genes group (1/0μM, 10/0μM, 50/0μM, 100/0μM and 500/0μM) exposed to 0 μg d^{-1} microplastic and 30 μg d^{-1} aSMPs. Venn analysis differentially expressed genes group (1/0μM, 10/0μM, 50/0μM, 100/0μM and 500/0μM) exposed to 0 μg d^{-1} microplastic (a) and 30 μg d^{-1} aSMPs (b). Principal component analysis (PCA) analysis of group (1/0μM, 10/0μM, 50/0μM, 100/0μM and 500/0μM) exposed to 0 μg d^{-1} microplastic (c) and 30 μg d^{-1} aSMPs (d).

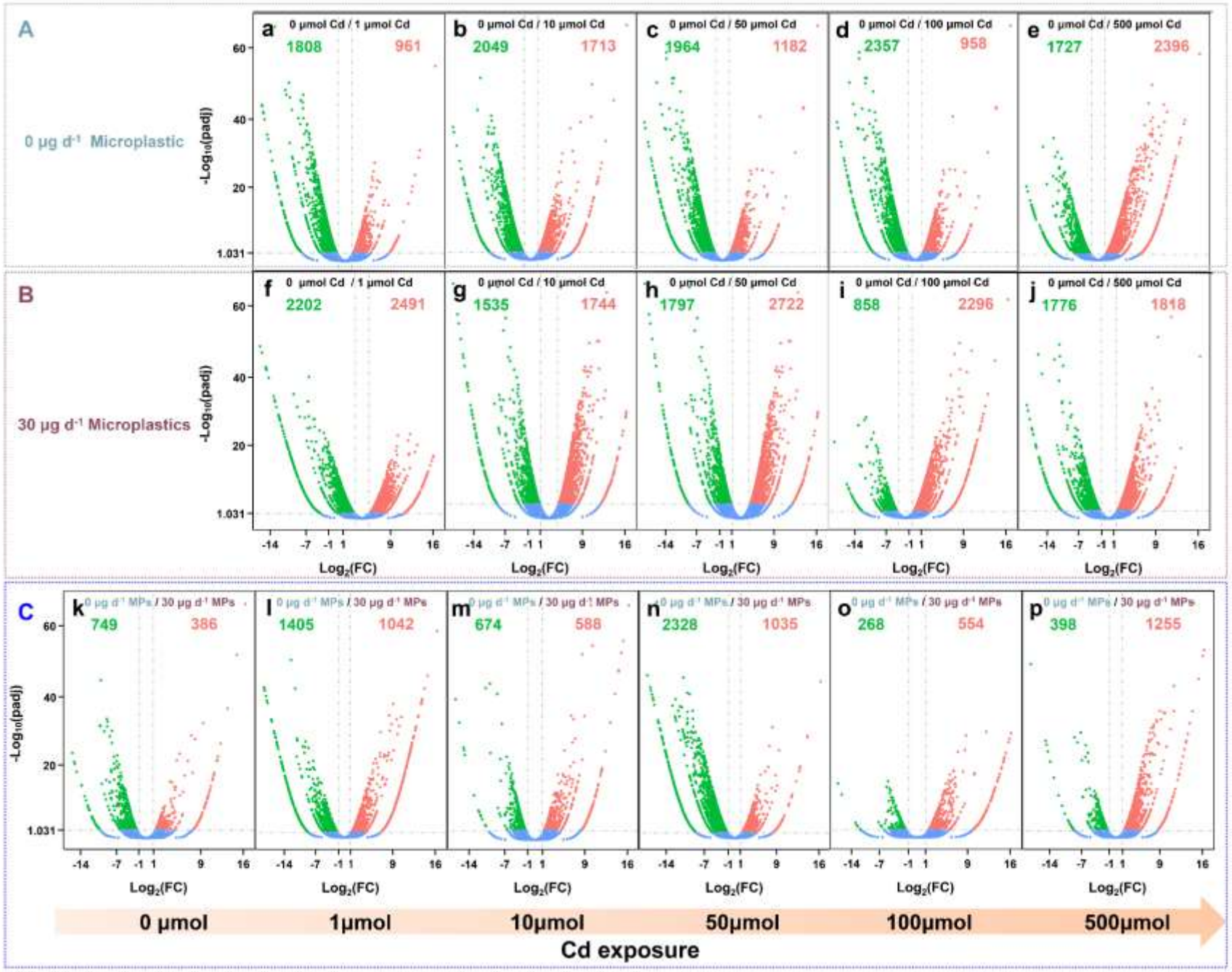
A
0 μg d-1 Microplastic
a 0 μmol Cd / 1 μmol Cd
1808
961
b 0 μmol Cd / 10 μmol Cd
2049
1713
c 0 μmol Cd / 50 μmol Cd
1964
1182
d 0 μmol Cd / 100 μmol Cd
2357
958
e 0 μmol Cd / 500 μmol Cd
1727
2396
B
30 μg d-1 Microplastics
f 0 μmol Cd / 1 μmol Cd
2202
2491
g 0 μmol Cd / 10 μmol Cd
1535
1744
h 0 μmol Cd / 50 μmol Cd
1797
2722
i 0 μmol Cd / 100 μmol Cd
858
2296
j 0 μmol Cd / 500 μmol Cd
1776
1818
-Log10(padj)
60
40
20
1.031
-14 -7 -1 1 9 16
Log2(FC)
C
k 0 μg d-1 MPs / 30 μg d-1 MPs
749
386
l 0 μg d-1 MPs / 30 μg d-1 MPs
1405
1042
m 0 μg d-1 MPs / 30 μg d-1 MPs
674
588
n 0 μg d-1 MPs / 30 μg d-1 MPs
2328
1035
o 0 μg d-1 MPs / 30 μg d-1 MPs
268
554
p 0 μg d-1 MPs / 30 μg d-1 MPs
398
1255
0 μmol
1μmol
10μmol
50μmol
100μmol
500μmol
Cd exposure

Figure S6. The volcano plots of differentially expressed genes group (1/0μM, 10/0μM, 50/0μM, 100/0μM and 500/0μM) exposed to 0 μg d^{-1} microplastic (A, a-e) and 30 μg d^{-1} aSMPs (B, f-j). The volcano plots of differentially expressed genes group (0 μg d^{-1} microplastic and 30 μg d^{-1} aSMPs) exposed with 0, 1, 10, 50, 100 and 500 μmol Cd (C,k-p). The red dots indicate that the genes were differentially expressed, and the blue dots indicate that the genes were not differentially expressed. The positive and negative values of Log_2 FC represent the up- and down-regulation of differentially expressed genes.

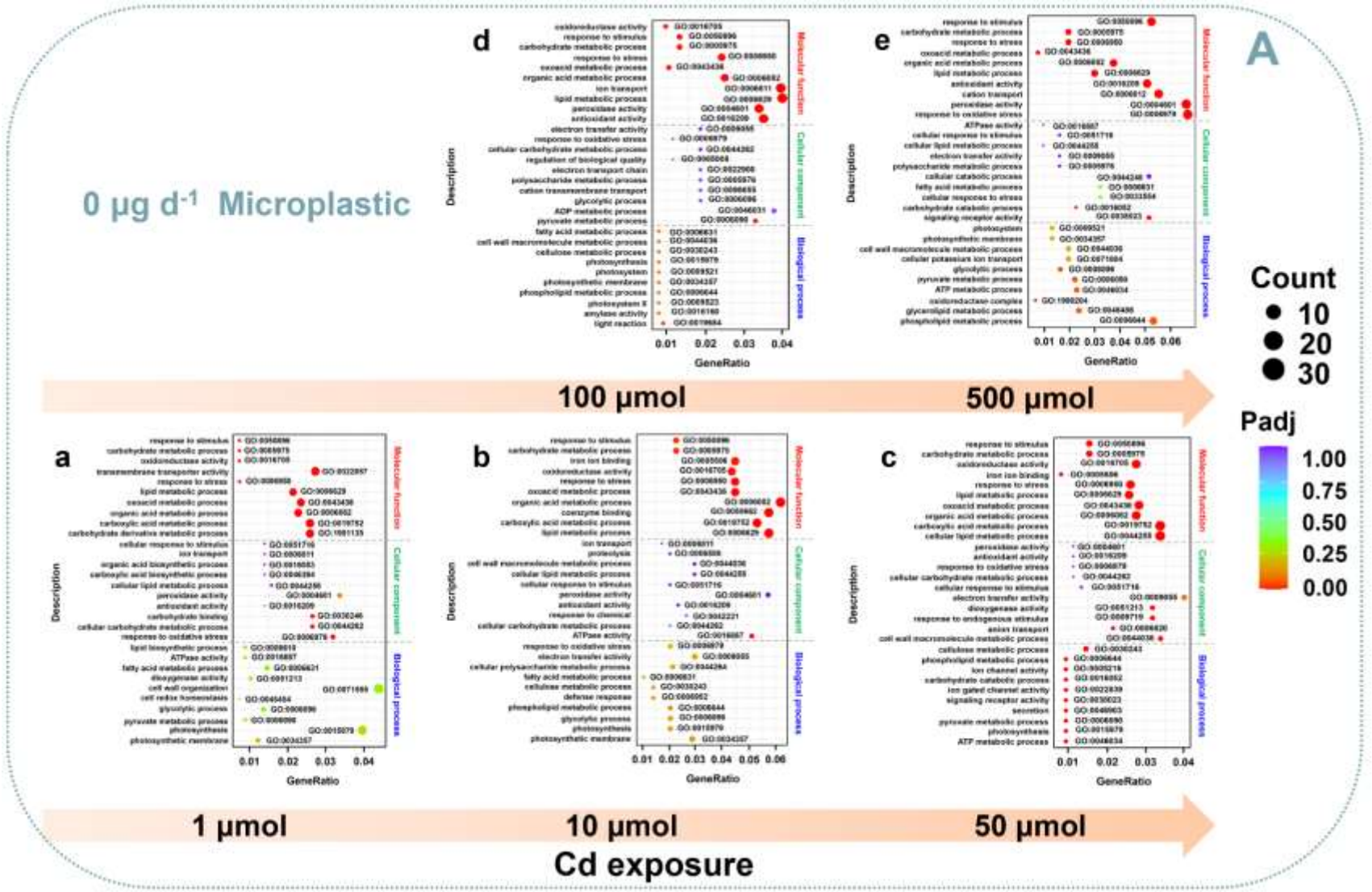
0 μg d-1 Microplastic
d
e
A
Count
10
20
30
Padj
1.00
0.75
0.50
0.25
0.00
100 μmol
500 μmol
a
b
c
1 μmol
10 μmol
50 μmol
Cd exposure
Description
GeneRatio
Molecular function
Cellular component
Biological process

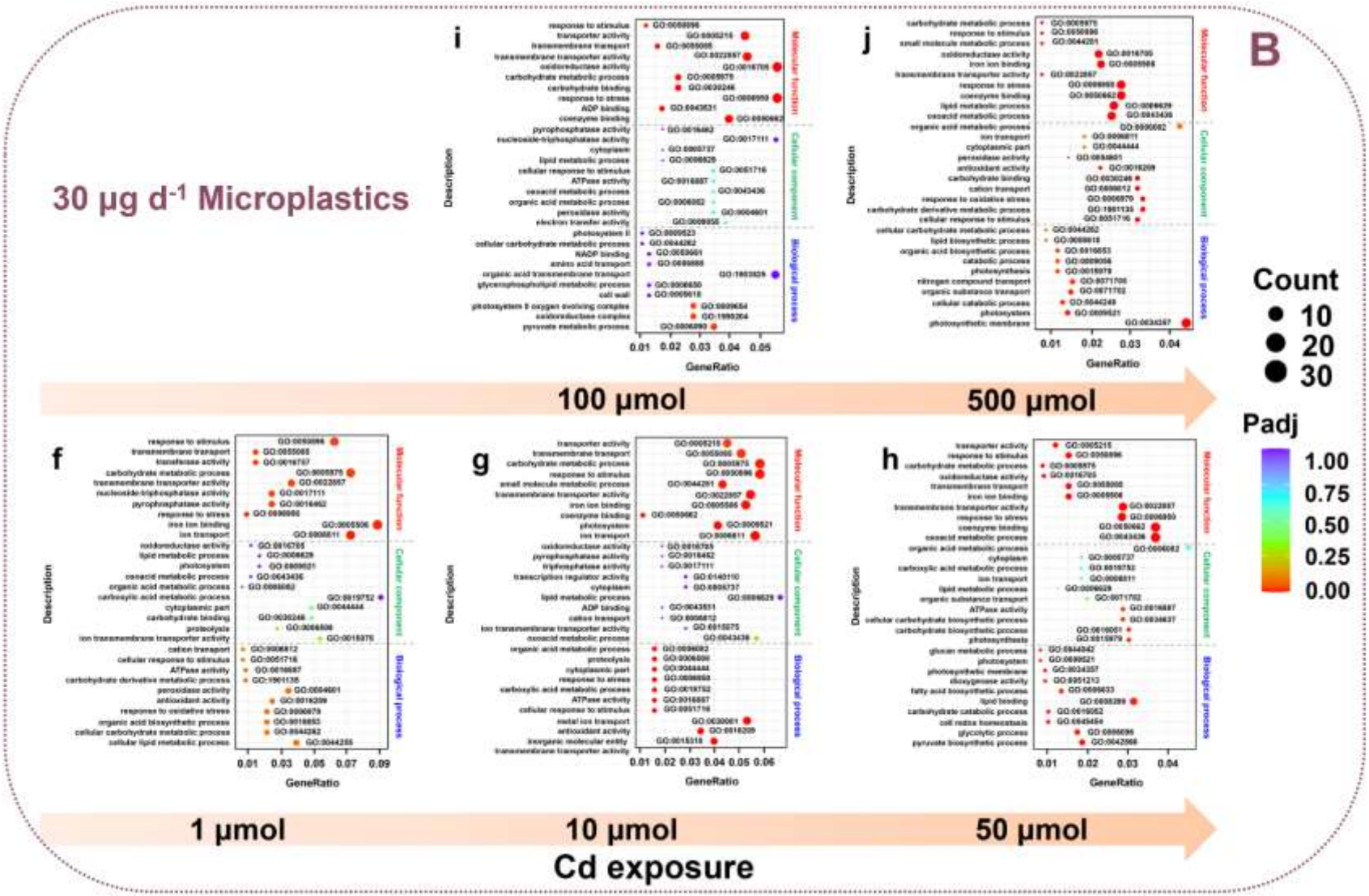
30 μg d-1 Microplastics
i
j
B
Count
10
20
30
Padj
1.00
0.75
0.50
0.25
0.00
Description
GeneRatio
Molecular function
Cellular component
Biological process
100 μmol
500 μmol
f
g
h
1 μmol
10 μmol
50 μmol
Cd exposure

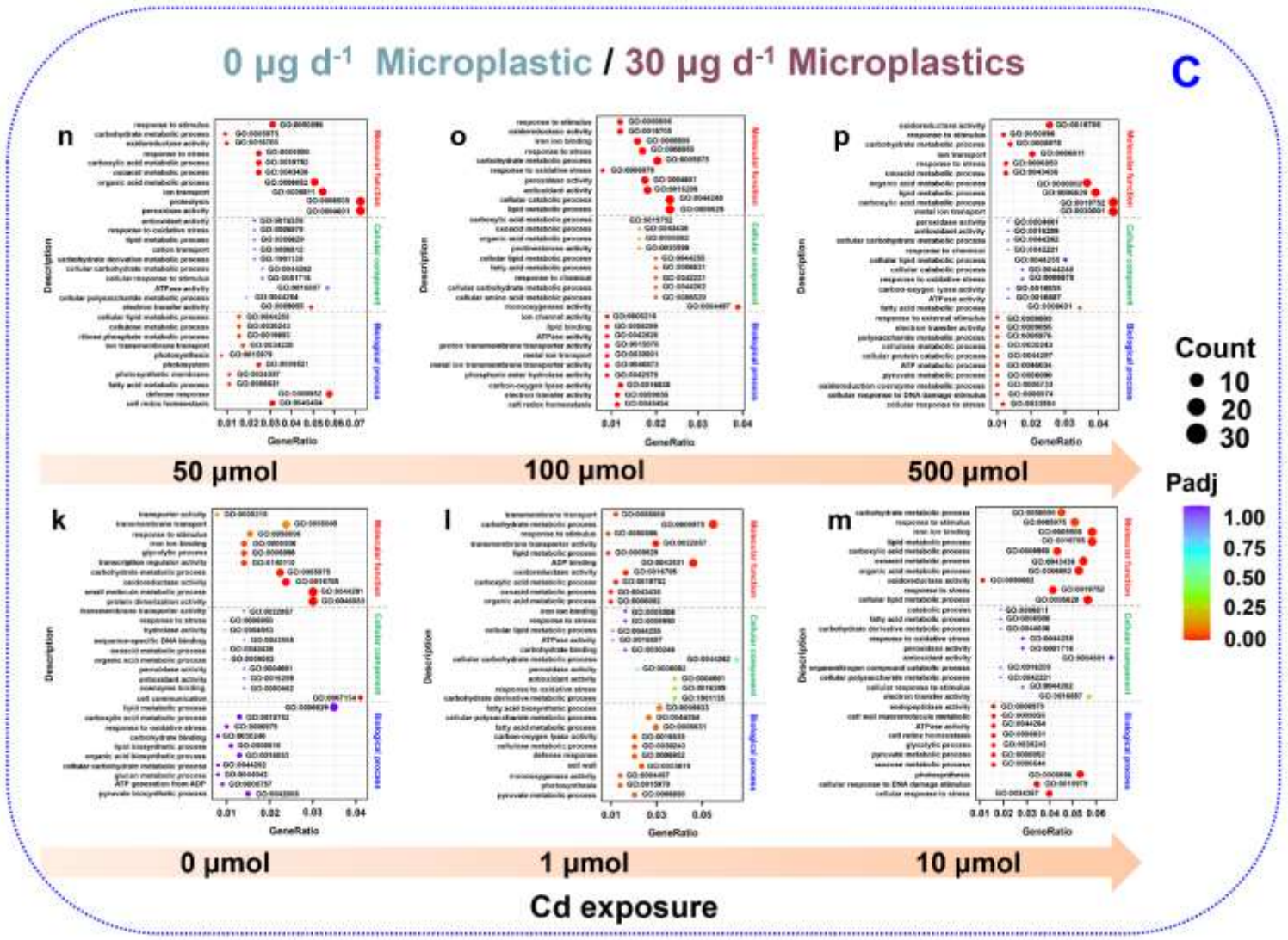
0 μg d-1 Microplastic / 30 μg d-1 Microplastics
C
n
o
p
Description
GeneRatio
50 μmol
100 μmol
500 μmol
Count
10
20
30
Padj
1.00
0.75
0.50
0.25
0.00
k
l
m
0 μmol
1 μmol
10 μmol
Cd exposure

Figure S7. Go enrichment analysis of differentially expressed genes group (1/0μM, 10/0μM, 50/0μM, 100/0μM and 500/0μM) exposed to 0 μg d^{-1} microplastic (A, a-e) and 30 μg d^{-1} aSMPs (B, f-j). Go enrichment analysis of differentially expressed genes group (0 μg d^{-1} microplastic and 30 μg d^{-1} aSMPs) exposed with 0, 1, 10, 50, 100 and 500 μmol Cd (C,k-p). The length of bars was determined by the log10 of the *p*-value. The numbers in every pathway represented the number of involved genes.

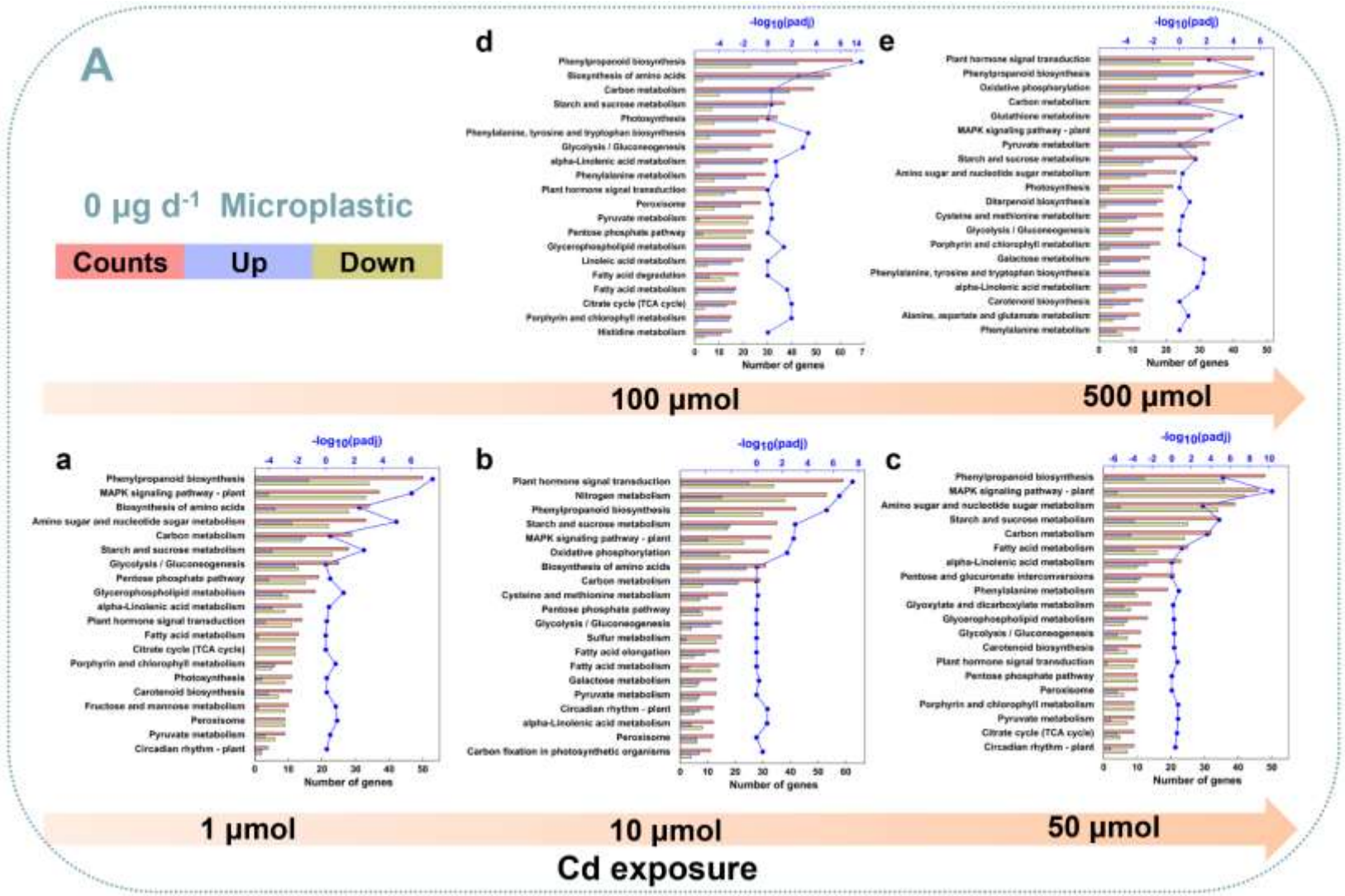
A
0 μg d-1 Microplastic
Counts
Up
Down
d
e
-log10(padj)
Number of genes
100 μmol
500 μmol
a
b
c
1 μmol
10 μmol
50 μmol
Cd exposure

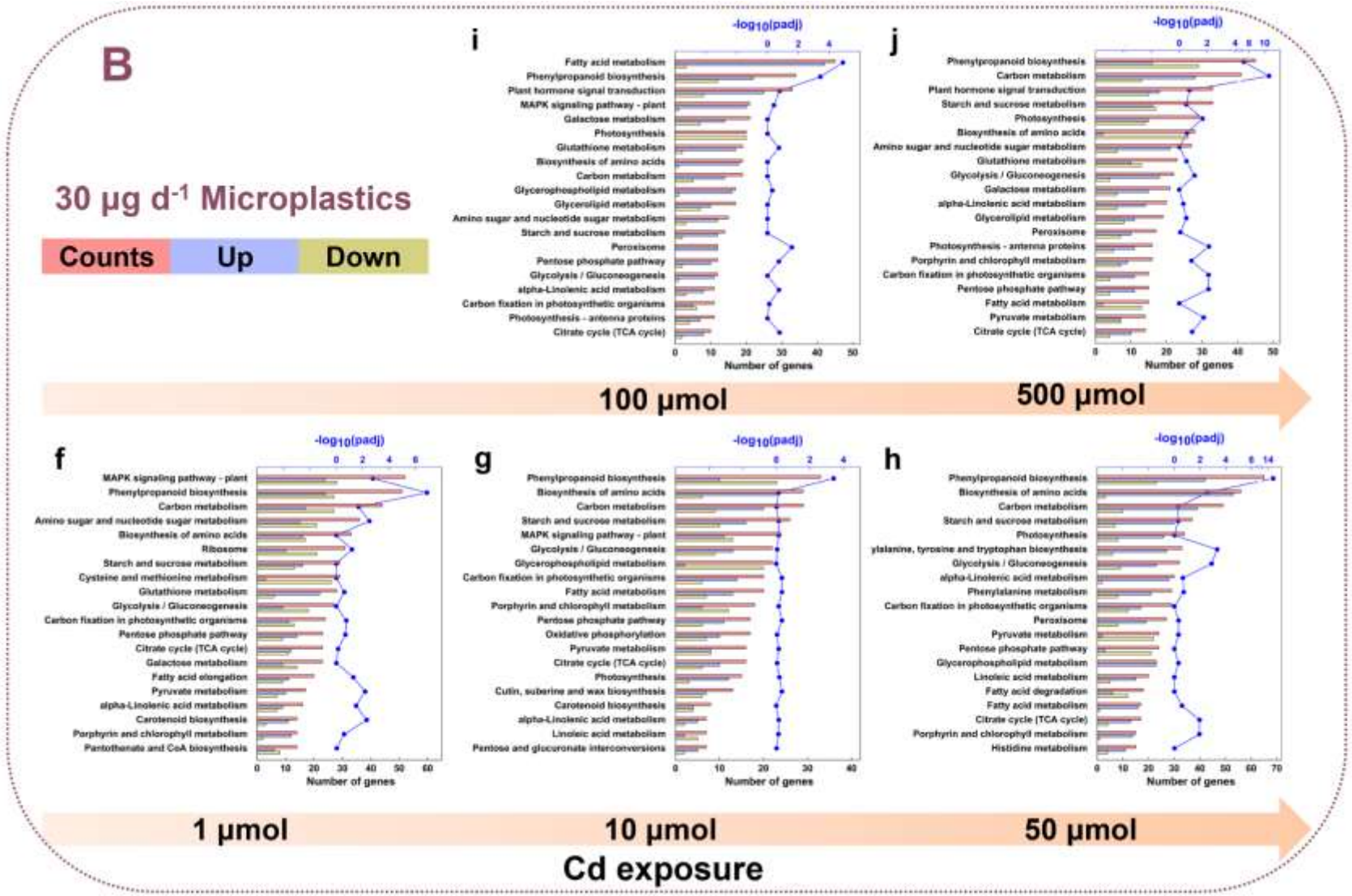
B
30 μg d-1 Microplastics
Counts
Up
Down
i
-log10(padj)
Fatty acid metabolism
Phenylpropanoid biosynthesis
Plant hormone signal transduction
MAPK signaling pathway - plant
Galactose metabolism
Photosynthesis
Glutathione metabolism
Biosynthesis of amino acids
Carbon metabolism
Glycerophospholipid metabolism
Glycerolipid metabolism
Amino sugar and nucleotide sugar metabolism
Starch and sucrose metabolism
Peroxisome
Pentose phosphate pathway
Glycolysis / Gluconeogenesis
alpha-Linolenic acid metabolism
Carbon fixation in photosynthetic organisms
Photosynthesis - antenna proteins
Citrate cycle (TCA cycle)
Number of genes
j
-log10(padj)
Phenylpropanoid biosynthesis
Carbon metabolism
Plant hormone signal transduction
Starch and sucrose metabolism
Photosynthesis
Biosynthesis of amino acids
Amino sugar and nucleotide sugar metabolism
Glutathione metabolism
Glycolysis / Gluconeogenesis
Galactose metabolism
alpha-Linolenic acid metabolism
Glycerolipid metabolism
Peroxisome
Photosynthesis - antenna proteins
Porphyrin and chlorophyll metabolism
Carbon fixation in photosynthetic organisms
Pentose phosphate pathway
Fatty acid metabolism
Pyruvate metabolism
Citrate cycle (TCA cycle)
Number of genes
100 μmol
500 μmol
f
-log10(padj)
MAPK signaling pathway - plant
Phenylpropanoid biosynthesis
Carbon metabolism
Amino sugar and nucleotide sugar metabolism
Biosynthesis of amino acids
Ribosome
Starch and sucrose metabolism
Cysteine and methionine metabolism
Glutathione metabolism
Glycolysis / Gluconeogenesis
Carbon fixation in photosynthetic organisms
Pentose phosphate pathway
Citrate cycle (TCA cycle)
Galactose metabolism
Fatty acid elongation
Pyruvate metabolism
alpha-Linolenic acid metabolism
Carotenoid biosynthesis
Porphyrin and chlorophyll metabolism
Pantothenate and CoA biosynthesis
Number of genes
g
-log10(padj)
Phenylpropanoid biosynthesis
Biosynthesis of amino acids
Carbon metabolism
Starch and sucrose metabolism
MAPK signaling pathway - plant
Glycolysis / Gluconeogenesis
Glycerophospholipid metabolism
Carbon fixation in photosynthetic organisms
Fatty acid metabolism
Porphyrin and chlorophyll metabolism
Pentose phosphate pathway
Oxidative phosphorylation
Pyruvate metabolism
Citrate cycle (TCA cycle)
Photosynthesis
Cutin, suberine and wax biosynthesis
Carotenoid biosynthesis
alpha-Linolenic acid metabolism
Linoleic acid metabolism
Pentose and glucuronate interconversions
Number of genes
h
-log10(padj)
Phenylpropanoid biosynthesis
Biosynthesis of amino acids
Carbon metabolism
Starch and sucrose metabolism
Photosynthesis
ylalanine, tyrosine and tryptophan biosynthesis
Glycolysis / Gluconeogenesis
alpha-Linolenic acid metabolism
Phenylalanine metabolism
Carbon fixation in photosynthetic organisms
Peroxisome
Pyruvate metabolism
Pentose phosphate pathway
Glycerophospholipid metabolism
Linoleic acid metabolism
Fatty acid degradation
Fatty acid metabolism
Citrate cycle (TCA cycle)
Porphyrin and chlorophyll metabolism
Histidine metabolism
Number of genes
1 μmol
10 μmol
50 μmol
Cd exposure

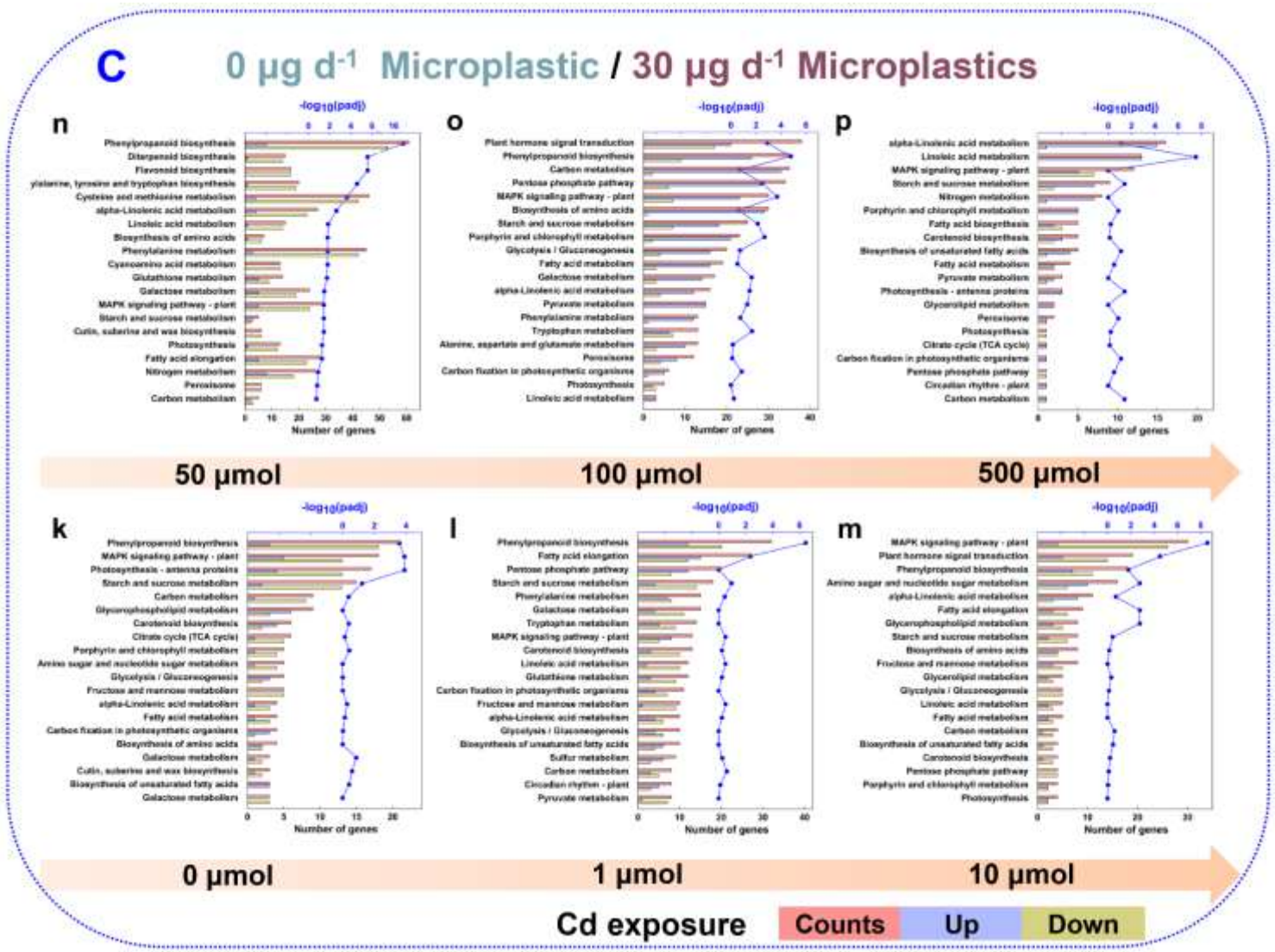
C
0 μg d-1 Microplastic / 30 μg d-1 Microplastics
n
o
p
-log10(padj)
Number of genes
50 μmol
100 μmol
500 μmol
k
l
m
0 μmol
1 μmol
10 μmol
Cd exposure
Counts
Up
Down

Figure S8. KEGG pathway analysis of differentially expressed genes group (1/0μM, 10/0μM, 50/0μM, 100/0μM and 500/0μM) exposed to 0 μg d^{-1} microplastic (A, a-e) and 30 μg d^{-1} aSMPs (B, f-j). KEGG pathway analysis of differentially expressed genes group (0 μg d^{-1} microplastic and 30 μg d^{-1} aSMPs) exposed with 0, 1, 10, 50, 100 and 500 μmol Cd (C,k-p). The length of bars was determined by the log10 of the p-value. The numbers in every pathway represented the number of involved genes.

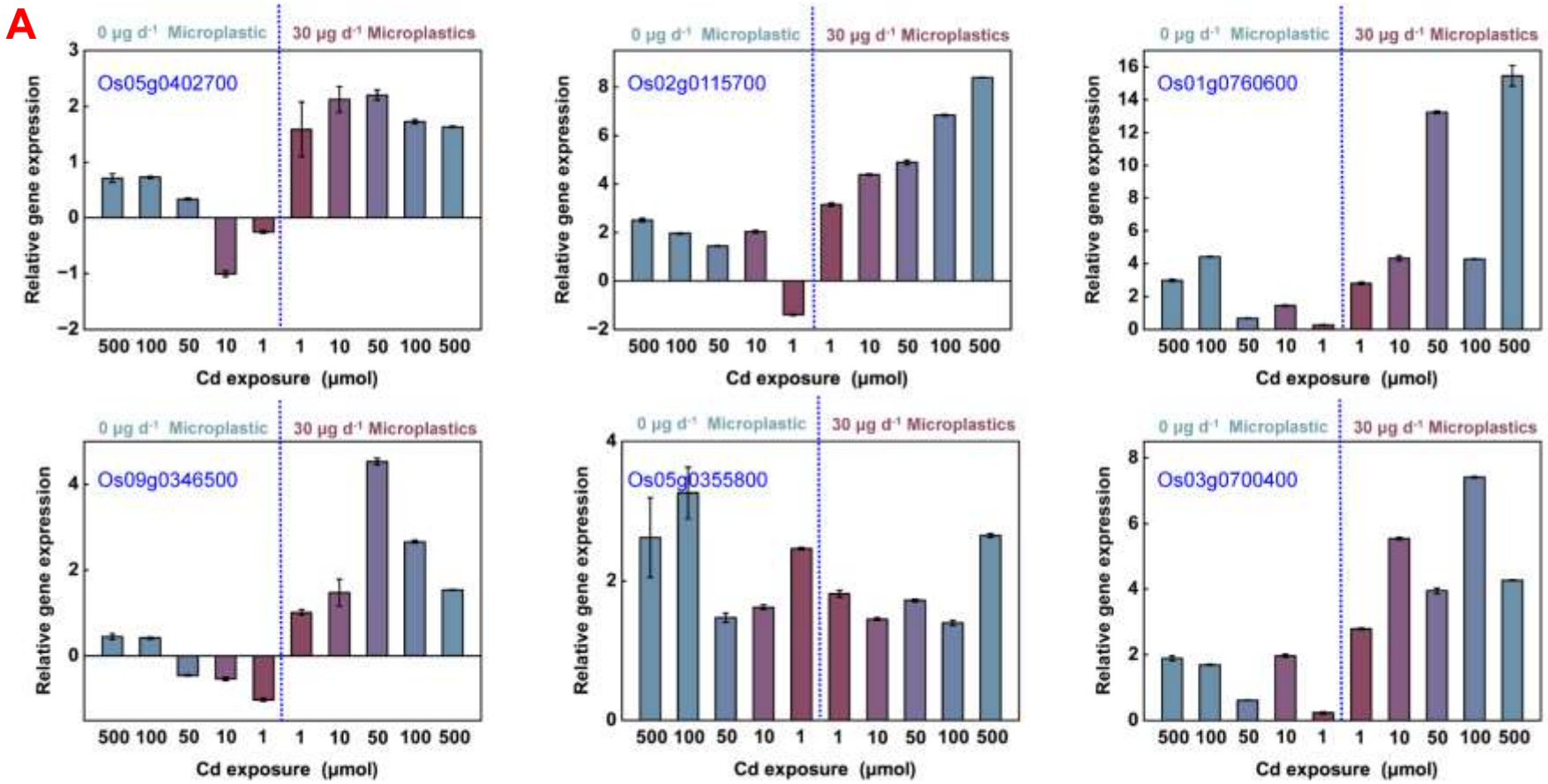
A
0 μg d⁻¹ Microplastic
30 μg d⁻¹ Microplastics
Os05g0402700
Os02g0115700
Os01g0760600
Os09g0346500
Os05g0355800
Os03g0700400
Relative gene expression
Cd exposure (μmol)
500 100 50 10 1 1 10 50 100 500

B

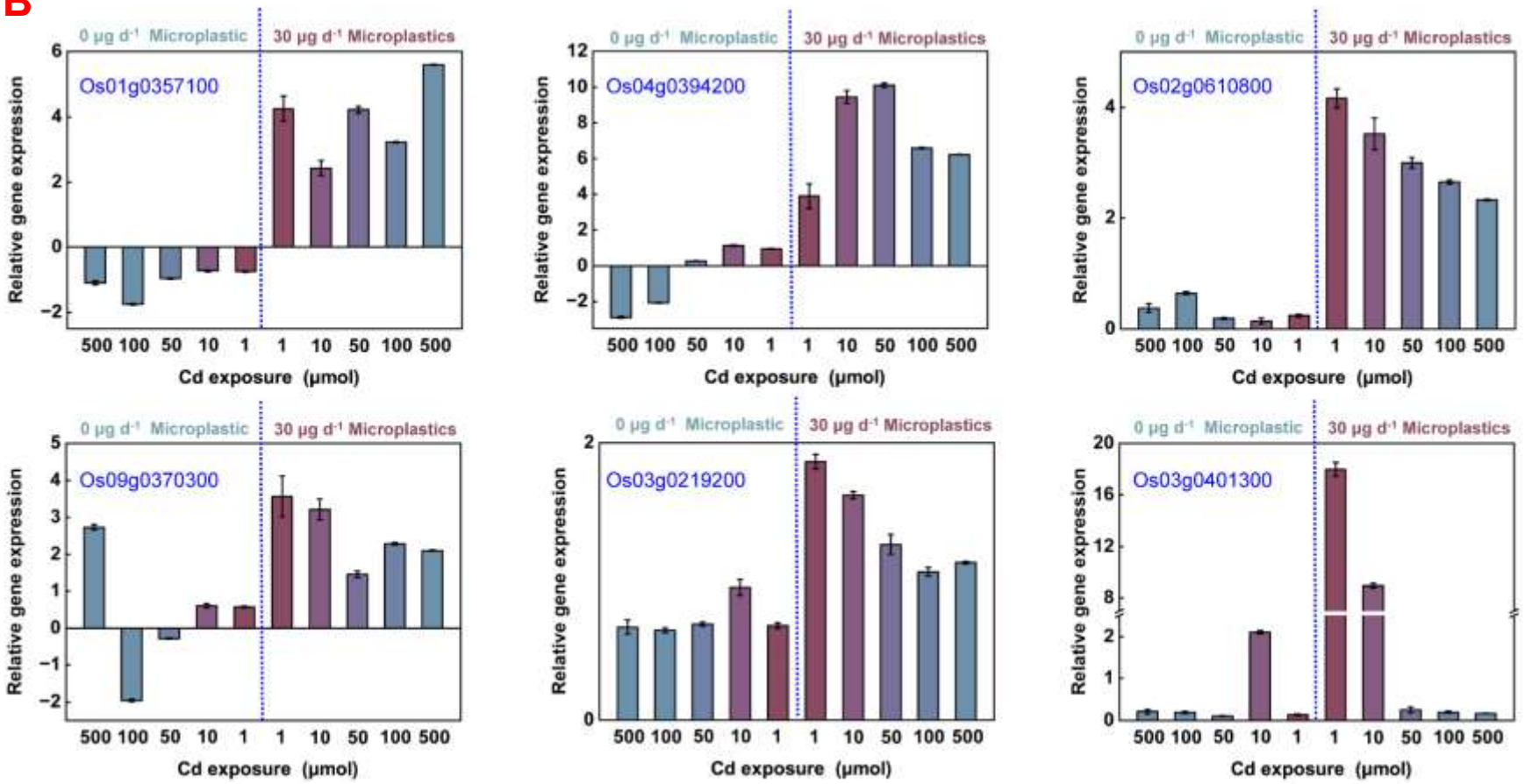
0 μg d⁻¹ Microplastic
30 μg d⁻¹ Microplastics
Os01g0357100
Os04g0394200
Os02g0610800
Os09g0370300
Os03g0219200
Os03g0401300
Relative gene expression
Cd exposure (μmol)
500 100 50 10 1 1 10 50 100 500

Figure S9. Real-time quantitative PCR (qPCR) validations of 12 selected differentially expressed genes group (1/0μM, 10/0μM, 50/0μM, 100/0μM and 500/0μM) exposed to 0 μg d^{-1} microplastic and 30 μg d^{-1} aSMPs. The heterogeneous nuclear ribonucleoprotein (HNR) was chosen as the internal reference gene.

Table S1. The relative content of metabolites detected in leaves of rice with 0 μg d^{-1} microplastic.

Serial	Category	Metabolite	Cd exposure (μmol)					
			0	1	10	50	100	500
m1		Citrulline	3.99	3.40	3.81	1.13**	1.30**	1.46**
m2		Glycine	313.88	128.47*	153.30*	155.54*	75.26**	30.24**
m3		L-Valine	3.40	2.85	3.98	2.47	6.06	3.78
m4		L-Glutamine	3.31	3.88	28.47**	6.27**	11.62**	5.11
m5		L-Proline	5.77	1.22**	4.23	1.12**	2.76*	0.87**
m6		L-Serine	13.55	9.43	31.94	11.95	26.11	12.96
m7		L-Threonine	3.00	1.60	0.64**	0.47**	1.57*	2.68
m8		Pyroglutamic acid	13.75	8.77	28.76	11.26	23.87	18.21
m9		L-Alanine	6.43	3.56	13.79	5.45	20.66*	4.34
m10		β.-Alanine	0.73	0.37	0.90	0.50	0.84	1.17
m11	Amino acid	L-Aspartic acid	30.24	14.26	71.19	17.33	35.32	19.95
m12		D-Asparagine	5.83	2.04*	10.69	1.99*	8.61	1.00**
m13		L-Asparagine	4.39	3.89	12.16	1.50*	31.06*	6.45
m14		γ-Aminobutyric acid	32.70	17.20	43.31	14.10*	12.29*	10.48*
m15		2-Aminoadipic acid	1.11	0.32	1.36*	0.96	1.06	2.15**
m16		L-Leucine	4.45	0.14**	0.64**	0.74**	3.80	0.87**
m17		L-Isoleucine	9.55	7.14	20.32*	7.89	41.66**	9.10
m18		L-Glutamic acid	19.33	11.95	73.60**	53.38**	80.42**	96.76**
m19		Canavanine	ND	ND	ND	ND	ND	ND
m20		N-Acetyl-L-alanine	6.03	3.96*	1.89*	0.49**	1.69**	3.57*
m21		L-Cystathionine	ND	ND	ND	ND	ND	ND

m22		Ornithine	13.99	11.39	11.48	3.36**	2.72**	2.08**
m23		L-Phenylalanine	1.48	0.59	2.31	0.46**	0.85	0.71*
m24	Carbohydrates	Sucrose	37.58	47.02	309.06	59.12	76.42	54.79
m25		D-Ribose	0.51	26.66**	52.82**	14.96**	3.26*	0.04*
m26		Pectin	12.48	4.12**	4.53**	3.25**	1.86**	1.27**
m27		D-Fructose	463.35	188.93*	584.90*	135.82*	114.14**	89.31**
m28		L-Arabinose	ND	ND	ND	ND	ND	ND
m29		Galacturonic acid	4.19	2.20	8.07**	1.86*	4.90	1.79*
m30		D-Mannose	ND	ND	ND	ND	ND	ND
m31		D-Galactose	36.25	4.25**	11.85**	1.27**	1.77**	2.27**
m32		D-Glucose	37.64	13.85*	40.41	9.74**	39.02	7.88**
m33		Lactulose	0.10	0.49**	0.88**	1.27**	1.66**	2.05**
m34		D-Cellobiose	6.21	1.57*	5.22	1.20**	0.74**	0.27**
m35		Maltose	14.45	6.81	49.32**	6.69*	4.99**	3.29**
m36		D-Arabinose	ND	ND	ND	ND	ND	ND
m37		Mannobiose	5.46	3.18	10.80**	2.18**	2.12**	14.10**
m38		D-Threitol	ND	ND	ND	ND	ND	ND
m39		Levoglucosan	8.26	8.74	10.76	4.03*	17.60**	7.35
m40		Erythrose	1.05	0.18**	1.28	0.12**	1.37	0.15**
m41		UDP- glucose	6.87	3.56*	11.07**	3.09**	18.59**	2.65**
m42		Sorbitol	4.27	0.52**	4.79	1.14**	1.79**	2.45**
m43		Xylulose	112.32	51.67**	260.75**	28.03**	27.99**	27.95**
m44		alpha-D-Allofuranose	ND	ND	ND	ND	ND	ND
m45		D-Xylose	ND	ND	ND	ND	ND	ND

m46		Boric acid	21.78	12.40*	43.38**	8.82**	18.21*	7.03**
m47		Ferulic acid	ND	ND	ND	ND	ND	ND
m48		Gluconic acid	50.31	31.36	94.77**	47.24	100.20**	28.77
m49		Citric acid	25.77	4.45**	31.57	4.82**	7.18**	9.54**
m50		Lactic Acid	9.48	5.39	10.42	4.70	15.16	12.37
m51		Salicylic acid	2.57	0.34**	2.88	0.56**	9.45**	3.06
m52		cis-p-Coumaric acid	0.73	0.71	0.64	0.79	0.56	0.64
m53		Dihydroxyacetone	0.74	0.41*	0.16**	0.25**	6.58**	4.96**
m54		Malic acid	64.19	20.58**	94.56**	22.14**	83.53*	52.07
m55		Glyceric acid	8.44	2.02**	6.71	2.19**	6.28	3.79**
m56		Succinic acid	4.41	1.70**	6.46*	2.09**	6.38*	4.05
m57		Phenylacetic acid	27.06	11.07*	35.18*	9.26*	13.15*	9.00*
m58	Organic acid	Azelaic acid	1.88	0.60**	2.81**	1.01	2.99**	1.78
m59		Ribonic acid	1.59	1.39	3.96**	6.02**	8.08**	9.37**
m60		Fumaric acid	2.08	0.91**	4.41**	1.14**	2.80	1.67*
m61		Malonic acid	0.65	0.22**	0.59	0.10**	0.69	0.17**
m62		Arabinonic acid	7.49	6.06	4.62*	3.19*	1.81**	0.26**
m63		Urea	2.32	2.49	5.70**	2.94	7.23**	5.69**
m64		Glycolic acid	0.83	0.36*	0.93	0.36*	1.56**	0.61
m65		Putrescine	3.66	1.33**	3.77	1.51**	2.05*	2.60*
m66		3-Aminoisobutanoic acid	0.70	0.47	2.29**	0.67	1.49*	1.68*
m67		Pentyl propanoate	0.30	0.33	0.37	0.37	0.43	0.48*
m68		Itaconic acid	0.37	2.10*	2.88**	3.98**	5.08**	6.18**
m69		Shikimic acid	29.85	12.67**	44.96**	13.83**	70.17**	15.44*
m70		Arachidic acid	27.31	46.84*	327.48**	81.94**	280.43**	48.13*

m71		Phosphite	0.74	0.44*	0.13**	1.02*	1.92*	0.33*
m72	Organic acid	Tyramine	24.94	0.90	0.66	1.39	2.11	4.93
m73		Hexyl 2E-hexenoate	0.09	0.06*	0.04**	0.02**	0.01**	0.03**
m74		Threonic acid	31.73	8.23*	18.93*	5.44**	11.95*	6.37**
m75		Stearic acid	8.29	6.07	10.94	5.12	17.16	6.12
m76		Ethanolamine	4.19	2.11	9.26*	2.86	3.45	8.30*
m77		Glycerol	3.10	2.27	9.69**	4.36	16.45**	8.43**
m78		1-Butylamine	1.67	0.67*	1.96	0.51**	6.33**	1.08
m79		Oleic acid	3.88	0.09**	0.09**	3.34	6.59**	9.84**
m80		MG(18:0/0:0/0:0)	19.49	7.41	21.93**	8.29**	30.79**	8.63**
m81	Fatty acid	Hydroxylamine	1.99	0.86*	4.97**	1.28	2.82**	3.04**
m82		Heptadecanoic acid	14.93	3.93*	3.53**	12.05	20.64*	29.23**
m83		Hydrocinnamic acid	1.65	0.48**	3.12**	0.66**	3.34**	0.35**
m84		Linoleic acid	46.70	11.82**	30.89*	10.70**	13.98**	13.31**
m85		Palmitic Acid	0.24	0.16	0.21	0.26	1.36**	0.47*
m86		Behenic acid	ND	ND	ND	ND	ND	ND
m87		Elaidic acid	ND	ND	ND	ND	ND	ND
m88		alpha-Linolenic acid	5.67	3.04*	13.37**	15.47**	19.53**	23.58**
m89		(R)-glycerol 1-acetate	ND	ND	ND	ND	ND	ND
m90		MG(16:0/0:0/0:0)	35.75	13.27**	41.07*	14.79**	59.11**	15.78**
m91		Glyceraldehyde	1.35	0.53**	0.39**	0.25**	0.44**	0.64*
m92		Petroselinic acid	8.14	2.22**	4.00*	2.62**	1.76**	0.90**
m93		Pentadecanoic acid	0.80	0.36**	1.78**	0.22**	0.29**	0.37*
m94	Polyols	Glycetate	0.53	0.45	1.92**	3.23**	4.54**	1.29*

m95		Polyethylene glycol	3.06	0.90**	8.49**	3.24	5.27	0.49**
m96		Stigmasterol	13.10	7.19	23.50	6.60	41.47	5.52
m97		Diethylene stearate	1.51	0.39**	1.27	0.86*	0.78**	0.69**
m98		Xylitol	135.02	55.28*	221.27	50.32*	157.52	57.99*
m99		D-Mannitol	1.08	0.56*	2.10*	2.27**	4.06**	4.31**
m100		Propylene glycol	0.13	0.76*	1.34**	1.94**	2.54**	3.14**
m101		1,2,3-Butanetriol	0.28	0.05**	0.48	0.16	1.35**	0.08**
m102		Erythritol	3.02	1.16**	2.76	8.44**	14.45**	0.65**
m103		1,3-Butanediol	0.12	1.22**	2.31**	0.04*	0.84**	0.80**
m104		beta-Mercaptoethanol	0.94	2.70**	4.47**	0.36	1.99*	1.94*
m105	Glycoside	Aucubin	0.68	0.68	0.99	1.29*	0.95	0.60
m106		Gluconolactone	9.93	9.45	22.83	9.41	13.11	5.80
m107	Vitamins	Myo-Inositol	3.23	0.63**	2.17	19.06**	55.72**	21.25**
m108	Nucleotide	Uridine	ND	ND	ND	ND	ND	ND
m109		Adenosine	10.25	3.45*	8.39	1.88**	1.29**	0.70**

*Significant difference when $p < 0.05$.

**Significant difference when $p < 0.01$.

ND: Not detected

Table S2. The relative content of metabolites detected in leaves of rice exposed with 30 μg d^{-1} aSMPs

Serial	Category	Metabolite	Cd exposure (μmol)					
			0	1	10	50	100	500
m1		Citrulline	1.63	7.24	1.72	1.83	1.93	2.09
m2		Glycine	3.31	2.24	3.07	4.17	5.85	6.84*
m3		L-Valine	4.96	1.98 **	5.08	6.34*	9.76*	11.67*
m4		L-Glutamine	22.96	4.28 **	9.26**	6.68**	6.19**	6.69**
m5		L-Proline	1.86	1.84	1.04**	1.12**	0.60**	0.62**
m6		L-Serine	15.49	6.81**	18.13	19.98	18.30	21.52*
m7		L-Threonine	21.48	4.22**	11.41**	11.60**	10.60**	12.31**
m8		Pyroglutamic acid	20.77	6.82**	14.01**	17.16	20.99	23.69
m9		L-Alanine	7.90	4.00**	9.28	8.87	9.32	11.79
m10		β.-Alanine	0.62	0.29**	0.36*	0.58	0.94	1.06*
m11	Amino acid	L-Aspartic acid	28.13	14.41**	14.51**	18.28**	18.77*	21.41*
m12		D-Asparagine	155.38	33.89**	81.13**	132.86	106.20*	117.45*
m13		L-Asparagine	ND	ND	ND	ND	ND	ND
m14		γ-Aminobutyric acid	18.06	18.62	13.91	15.82	17.21	19.76
m15		2-Aminoadipic acid	0.41	0.31*	1.22**	2.07**	2.39**	2.62**
m16		L-Leucine	3.30	2.27	2.78	3.07	6.05**	8.12**
m17		L-Isoleucine	8.50	2.09**	4.72**	6.52*	9.36	11.59*
m18		L-Glutamic acid	25.53	12.64**	6.84**	2.24**	9.48**	17.64**
m19		Canavanine	0.30	4.71**	0.49*	3.15**	3.81**	4.47**
m20		N-Acetyl-L-alanine	ND	ND	ND	ND	ND	ND
m21		L-Cystathionine	0.27	0.34	0.40	0.06**	0.29	0.31

m22	Amino acid	Ornithine	3.09	2.42	1.88	4.18	3.08	3.39
m23		L-Phenylalanine	3.42	9.76**	16.11**	22.13**	26.58**	30.56**
m24	Carbohydrates	Sucrose	15.96	41.58**	73.64**	174.71**	94.05**	111.41**
m25		D-Ribose	0.50	1.11	1.73	2.95*	0.19**	1.77**
m26		Pectin	11.21	0.57**	4.55*	7.36	4.43*	4.60*
m27		D-Fructose	278.93	224.34	137.78**	137.57**	144.26*	169.24
m28		L-Arabinose	27.66	10.31**	12.01**	24.94	15.33	50.14**
m29		Galacturonic acid	2.26	2.56	1.55	1.82	1.47**	1.53
m30		D-Mannose	0.21	0.26*	0.31**	0.33**	0.43**	0.43**
m31		D-Galactose	1.86	14.31**	0.61**	0.68**	1.04**	1.16**
m32		D-Glucose	12.43	113.73**	119.17**	124.60**	173.15**	205.41**
m33		Lactulose	ND	ND	ND	ND	ND	ND
m34		D-Cellobiose	3.15	1.67*	1.48*	2.21	1.12**	1.20**
m35		Maltose	7.46	20.68**	7.28	6.99	7.48	7.80
m36		D-Arabinose	0.83	0.58*	1.51**	2.43**	0.02**	1.15**
m37		Mannobiose	1.18	2.70**	6.79**	6.80**	6.38**	6.94**
m38		D-Threitol	0.08	0.32**	0.64**	0.55**	1.24**	1.24**
m39		Levoglucosan	3.37	0.61	0.45	1.01	1.33	1.19
m40		Erythrose	0.42	0.43	0.44	0.47	0.58	0.55
m41		UDP- glucose	3.62	3.09	3.50	3.64	3.35	3.79
m42		Sorbitol	1.17	0.85**	1.26	0.94	1.18	1.24
m43		Xylulose	77.05	40.08*	21.14**	51.86	69.45	69.00
m44		alpha-D-Allofuranose	0.44	0.53*	0.63*	1.06**	0.10**	0.10**
m45		D-Xylose	2.22	2.07	3.54**	0.08**	0.63**	2.56

m46		Boric acid	3.65	0.57**	1.36**	3.64	1.68*	1.92*
m47		Ferulic acid	0.23	0.20	0.12**	0.23	0.07**	0.07**
m48		Gluconic acid	30.20	27.66	34.31	47.53**	41.76**	47.87**
m49		Citric acid	14.15	10.90	2.53**	4.42**	6.59**	6.93**
m50		Lactic Acid	6.09	5.28	5.10	4.94	9.06	10.45
m51		Salicylic acid	0.83	0.67	0.78	0.53**	0.53**	0.46**
m52		cis-p-Coumaric acid	0.32	0.54*	0.82**	0.89**	1.22**	1.43**
m53		Dihydroxyacetone	0.62	0.47	0.44**	0.50*	0.13**	0.13**
m54		Malic acid	30.99	32.72	34.45	36.18*	36.51	38.87*
m55		Glyceric acid	2.37	2.37	2.12	3.68	4.09*	4.76*
m56		Succinic acid	1.57	2.50	1.69	3.42**	4.99**	5.78**
m57		Phenylacetic acid	0.25	0.23	0.21*	0.18*	0.16*	0.18*
m58	Organic acid	Azelaic acid	0.75	0.59	0.86	1.43*	1.79*	2.01**
m59		Ribonic acid	0.63	0.70	0.68	1.50	3.56**	4.28**
m60		Fumaric acid	1.15	0.92	0.95	0.53*	2.12**	2.12**
m61		Malonic acid	0.25	0.17	0.21*	0.16*	0.16*	0.16*
m62		Arabinonic acid	ND	ND	ND	ND	ND	ND
m63		Urea	3.97	1.77*	3.88	4.25	5.54	6.29
m64		Glycolic acid	0.37	0.36	0.37	0.62*	0.77*	0.92*
m65		Putrescine	1.77	1.18	1.73	1.97	1.87	2.17
m66		3-Aminoisobutanoic acid	0.37	0.64	0.54	0.70**	0.79**	0.88**
m67		Pentyl propanoate	ND	ND	ND	ND	ND	ND
m68		Itaconic acid	0.33	0.08**	0.11**	0.60	0.76*	0.94*
m69		Shikimic acid	1.93	4.43**	3.15*	4.41**	5.03**	5.65**
m70		Arachidic acid	0.27	0.31	0.40**	0.33*	0.44*	0.51*

m71		Phosphite	0.32	0.31	0.21**	0.48	0.21**	0.23**
m72		Tyramine	1.39	0.80*	0.90*	1.00**	0.80*	0.71**
m73	Organic acid	Hexyl 2E-hexenoate	0.03	0.06**	0.04*	0.07**	0.08**	0.09**
m74		Threonic acid	5.10	8.20	5.49	4.47	5.81	7.03
m75		Stearic acid	6.56	3.30**	6.37	7.95	7.59	9.36
m76		Ethanolamine	12.46	10.44	13.67	16.12*	27.00**	15.34
m77		Glycerol	21.84	14.89	6.78**	11.83*	13.91	15.34
m78		1-Butylamine	1.55	0.63**	0.60**	1.10	0.91*	1.14
m79		Oleic acid	2.94	0.13**	3.07*	6.01**	5.90**	7.04**
m80		MG(18:0/0:0/0:0)	21.15	7.99**	8.76**	13.67*	12.59**	13.99*
m81	Fatty acid	Hydroxylamine	2.48	2.03	1.25	6.44*	8.60*	11.41**
m82		Heptadecanoic acid	0.26	0.23	0.59**	0.82**	0.69**	0.78**
m83		Hydrocinnamic acid	0.64	1.15*	3.22**	3.56**	3.19**	5.03**
m84		Linoleic acid	2.01	2.85	2.09	3.27*	1.97	2.35
m85		Palmitic Acid	20.28	13.15*	16.45	26.39	23.45	29.92
m86		Behenic acid	0.27	0.25	0.22	0.25	0.16*	0.17*
m87		Elaidic acid	4.06	0.46**	4.52	0.50**	0.81**	0.21**
m88		alpha-Linolenic acid	3.00	3.90	3.50	3.10	3.52	3.58
m89		(R)-glycerol 1-acetate	0.34	0.49	0.42	0.36	0.22	0.26
m90		MG(16:0/0:0/0:0)	39.14	13.29**	14.01**	23.83*	22.53*	25.31*
m91		Glyceraldehyde	0.85	0.80	0.76	0.67	0.62	0.55*
m92		Petroselinic acid	4.05	3.40	2.74*	2.08*	1.43**	1.53**
m93		Pentadecanoic acid	0.61	0.38	0.34*	0.45	0.56	0.64
m94	Polyols	Glycetate	0.50	0.46	0.42	1.09*	1.76**	2.00**

m95		Polyethylene glycol	4.09	1.50**	1.63**	1.45**	0.99**	1.07**
m96		Stigmasterol	7.50	5.86	7.20	8.51	7.58	8.58
m97		Diethylene stearate	0.81	0.55	0.50*	0.47*	0.33**	0.24**
m98		Xylitol	103.33	59.95*	53.40*	91.79	93.12	111.61
m99		D-Mannitol	1.96	0.29**	0.85*	0.86*	0.36**	0.10**
m100		Propylene glycol	ND	ND	ND	ND	ND	ND
m101		1,2,3-Butanetriol	0.77	0.22**	0.10**	0.42**	0.79	1.16*
m102		Erythritol	3.37	0.91**	2.02**	0.82**	0.73**	0.76**
m103		1,3-Butanediol	ND	ND	ND	ND	ND	ND
m104		beta-Mercaptoethanol	ND	ND	ND	ND	ND	ND
m105	Glycoside	Aucubin	ND	ND	ND	ND	ND	ND
m106		Gluconolactone	6.78	9.58	7.88	9.69	11.71**	10.56
m107	Vitamins	Myo-Inositol	14.51	11.27	9.19*	10.08*	11.96	13.77
m108	Nucleotide	Uridine	1.66	2.56	0.20**	0.33**	0.25**	0.82**
m109		Adenosine	4.75	5.23	2.21**	1.49**	0.80**	0.80**

*Significant difference when $p < 0.05$.

**Significant difference when $p < 0.01$.

ND: Not detected

Table S3. Detailed information for the differentially expressed genes presented in the heatmap of Figure 5.

Gene ID	Symbol	Cd exposure+0 μg d^{-1} aSMPs						Cd exposure+30 μg d^{-1} aSMPs						Description
		0μM	1μM	10μM	50μM	100μM	500μM	0μM	1μM	10μM	50μM	100μM	500μM	
Glycolysis metabolism														
Os03g0401300	SS	0.14	2.44	0.17	0.32	0.36	11.23	5.53	0.18	0.14	0.10	0.14	2.44	Sucrose synthase 2 (EC 2.4.1.13)
Os05g0402700	ALDO	0.47	1.07	0.65	1.12	1.09	0.93	1.11	1.20	1.62	0.99	0.47	1.07	fructose-bisphosphate aldolase, class I [EC:4.1.2.13]
TCA cycle														
Os09g0370300	SDH3-2	1.02	1.21	0.31	3.08	4.29	1.99	1.78	1.36	1.36	2.07	1.02	1.21	succinate dehydrogenase (ubiquinone) iron-sulfur subunit [EC:1.3.5.1]
Os04g0394200	OADH	1.02	1.21	0.31	3.08	4.29	3.88	4.89	8.58	3.78	5.99	1.02	1.21	2-oxoglutarate dehydrogenase E2 component [EC:2.3.1.61]

Amino acid metabolism														
Os01g0357100	NIR	1.24	0.82	1.20	2.47	1.55	2.29	2.01	3.39	2.13	3.96	1.24	0.82	ferredoxin-nitrite reductase [EC:1.7.7.1]
Os01g0760600	GOT1	0.46	1.75	0.89	5.51	3.70	2.57	2.30	6.82	2.42	8.53	0.46	1.75	aspartate aminotransferase, cytoplasmic [EC:2.6.1.1]
Photosynthetic metabolism														
Os02g0610800	*psa*B	0.31	0.24	0.36	0.67	0.39	2.15	2.51	1.50	1.76	1.58	0.31	0.24	*psa*B translation factor, putative, expressed
Os09g0346500	LHC	1.06	0.78	0.88	0.66	0.71	0.40	0.90	2.54	1.86	1.18	1.06	0.78	light-harvesting complex II chlorophyll a/b binding protein 1
Fatty acid metabolism														
Os05g0355800	LOX	2.75	2.87	2.75	3.99	3.20	1.05	0.78	1.02	0.75	1.70	2.75	2.87	Glycine and cysteine rich family protein precursor, expressed
Os03g0700400	LOX1	0.05	2.58	0.84	3.36	3.75	1.68	2.82	2.25	3.98	2.26	0.05	2.58	lipoxygenase [EC: 1.13.11.12]

Antioxidative system														
Os02g0115700	CAT-A	4.66	7.12	4.64	5.99	7.86	1.61	1.98	2.51	3.02	7.74	4.66	7.12	catalase [EC:1.11.1.6]
Os03g0219200	SOD-4	1.28	0.97	0.87	0.73	0.76	1.09	0.90	0.66	0.73	0.82	1.28	0.97	superoxide dismutase, Cu-Zn family [EC:1.15.1.1]

In Figure 5, SS, ALDO, SDH, OADH, NIR, GOT, psaB, LHC, LOX, CAT and, SOD were the abbreviations of sucrose synthase, fructose-bisphosphate aldolase, succinate dehydrogenase iron-sulfur subunit 2, dihydrolipoyllysine-residue succinyl transferase, nitrite reductase, aspartate aminotransferase, photosystem I P700 chlorophyll a apoprotein A2, light-harvesting complex II chlorophyll a/b binding protein 6, linoleate 13S-lipoxygenase, catalase isozyme and superoxide dismutase.

Table S4. Primers used in the investigation the expression of 12 selected genes for the validation of transcriptomic analysis by an RT-qPCR approach.

Gene ID	Symbol	Forward prime (5′–3′)	Reverse primer (5′–3′)
Os03g0401300	SS	ATTGTAGCATCCTTGTTTCCAAGA	ATGCACAGTAAGGATTTCGAT
Os05g0402700	ALDO	CACGCTCCGAGAGCCTTC	CACATTAAGCAACAGCCGCA

Os09g0370300	SDH3-2	CAGTACAAGTCGGTGGAGCC	AGAATGCACTCGTACAGCCC
Os04g0394200	OADH	TCAAAGCTTACAAGAAGACGCT	TCACCCATGAAAGGGACAACA
Os01g0357100	NIR	ATCACCAGCAACTTCCAGGG	GAGGTCGTTGATGTGTGGGT
Os01g0760600	GOT1	TGGACTGGATTTCCAAGGGC	CCACTGGTCCAAAGTTGGGT
Os02g0610800	psaB	CCAGGAGAACCTCAACTCCG	AACACACGCTGCTAGATGCT
Os09g0346500	LHC	GACCGTAGCTTAGCAGTGGTT	CGATCATCATCTCGTCGCAC
Os05g0355800	LOX	TGACTGTCATCGACACGCTG	GACAGCCGGACTACACCAAC

Gene ID	Symbol	Forward prime (5′–3′)	Reverse primer (5′–3′)
Os03g0700400	LOX1	TCGATCCTAGCAAGTTCGGC	GTCCAGAATGTACAGCCGGT
Os02g0115700	CAT-A	GGACGAGGAGGTGGACTACT	TGCTTGTGTATCGTCGCCTT
Os03g0219200	SOD-4	TCCACATCCACTCCTTTGGC	AGGTCGCCCACATGTCTTTC